J. Fluid Mech. (1991), *vol.* 225, *pp.* 301–331
Printed in Great Britain

Laboratory experiments on the tripolar vortex in a rotating fluid

By G. J. F. VAN HEIJST, R. C. KLOOSTERZIEL† AND C. W. M. WILLIAMS

Institute of Meteorology and Oceanography, University of Utrecht, Princetonplein 5, 3584 CC Utrecht, The Netherlands

(Received 14 March 1990 and in revised form 24 September 1990)

Within the framework of the study of coherent vortex structures as emerging in rotating, quasi-two-dimensional flows, the tripolar vortex is a relatively novel feature. It consists of a symmetric, linear arrangement of three patches of distributed vorticity of alternate signs, and the axis of this configuration rotates about the centre of the core vortex. This paper describes an experimental study of the formation of a tripole from an unstable axisymmetric vortex in a solidly rotating, homogeneous fluid. The flow is visualized by addition of dye, and is measured by streak photography of tracer particles. After digitization, the spatial distributions of the vorticity ω and the stream function ψ are calculated numerically, and 'scatter plots' of ω versus ψ are presented for the various stages in the tripole formation process. Owing to viscous effects (spin-down by the bottom Ekman layer and lateral entrainment of ambient fluid) the tripole shows an exponential decay, both in its rotation speed and its internal, relative flow. The comparison of the observed flow characteristics with a simple point-vortex model shows reasonable quantitative agreement.

1. Introduction

In contrast to three-dimensional turbulence, quasi-geostrophic or two-dimensional turbulence is characterized by a spectral flux of kinetic energy to larger scales of motion, usually referred to as the 'inverse energy cascade'. Phenomenologically, this is recognized in the emergence of coherent vortex structures from an initial state of randomly distributed vorticity. Two well-known types of coherent structures are (i) the single, circularly symmetric vortex ('monopole') and (ii) the dipole, consisting of two closely packed counter-rotating vortices. The monopolar vortex has a non-zero angular momentum (if the swirl velocity is of the same sign everywhere), and – in the absence of any background flow, forcing and dissipation – it will be stationary in space. On the other hand, the vorticity distribution of the vortex dipole provides a *self-propelling* mechanism to this structure, which causes the dipole to propagate steadily in a direction defined by its axis of symmetry. In other words, the dipole is characterized by a non-zero linear momentum, while its angular momentum is zero.

Because of its relevance to large-scale geophysical flow systems, the dynamics of two-dimensional turbulence have been studied by an increasing number of investigators during the last decade. In particular the advent of powerful supercomputers made numerical simulations of this type of turbulence possible. For example, McWilliams (1984) describes the emergence of coherent vortex structures

† Present affiliation: Institute for Nonlinear Science (INLS), La Jolla, CA 92093, USA.

in the numerically simulated viscous evolution of a two-dimensional flow from an initial state of randomly distributed vorticity: in these calculations the vorticity is observed to eventually become concentrated in isolated patches which show a gradual relaxation towards axisymmetry. Similar 'monopolar' vortices were also found in later numerical simulations with higher resolution, see e.g. Sadourny (1985), Benzi, Patarnello & Santangelo (1987, 1988) and Legras, Santangelo & Benzi (1988). These studies revealed that – in addition to vortex monopoles – dipolar vortices can emerge equally well during the evolution of the flow.

Moreover, Legras *et al.* (1988) observed the emergence of a tripolar vortex structure in their numerical simulation of the flow evolving from an initial state of randomly distributed vorticity. This tripole consists of a compact linear arrangement of three patches of distributed vorticity: the central vortex has an elliptical shape and is adjoined at its longer sides by two weaker satellite vortices of signs opposite to that of the core vortex. The axis of alignment rotates about the centre of the vortex structure, in the same sense as the rotation in the core. By inspecting the literature (as described in some detail by Kloosterziel & van Heijst 1989), a few other examples of tripolar vortices were found that had not been explicitly referred to before. In a numerical study of the evolution of circular two-layer Gaussian rings, for instance, Ikeda (1981) observed that perturbations corresponding to slightly elliptical (wavenumber 2) deformation of the initial vortex could under certain circumstances result in a tripolar vorticity structure. Similar features were also found by Swenson (1987) in a numerical study of unstable monopolar vortices. These results were not recognized as being associated with the tripole as a novel coherent structure, whose explicit existence was described only recently in the paper of Legras *et al.* (1988).

Independent of this numerical discovery of the tripole, laboratory experiments on barotropic vortices in a rotating fluid were carried out by the present authors, and these experiments confirmed the existence of the tripolar vortex in the real, physical world: under certain conditions barotropic vortices can become unstable, and show a gradual transition into a rotating vortex tripole. Its existence was first observed (by chance) in experiments carried out in 1984, but this experimental evidence of the tripole occurring as a stable vortex structure in a (quasi) two-dimensional flow was not published until 1989 (van Heijst & Kloosterziel 1989 and Kloosterziel & van Heijst 1989).

In the meantime, other numerical modellers performed detailed simulations of the instability of perturbed monopolar vortices, and this work provided more detailed information about the vorticity distribution within the vortex during its evolution towards the ultimate, stable tripolar state (Carton, Flierl & Polvani 1989). Their numerical results appear to agree very well with the observations of the 'real' tripole as described by van Heijst & Kloosterziel (1989) and Kloosterziel & van Heijst (1989). The present paper is a continuation of the work reported in those papers, and presents more detailed characteristics of the tripolar vortex as measured in the laboratory experiments. The experimental technique as well as some general observations of the tripole formation are described in §2. Quantitative information about the vortex was obtained by digitizing the flow field, and §3 contains results of the observed spatial distributions of important flow properties such as the vorticity and stream function, as well as the observed tripole rotation speed, and the gradual decay of the tripole due to viscous effects. Although at this stage no complete analytical model of the tripolar vortex has been developed, a simple point-vortex model is described in §4, which appears to capture fairly well the overall rotation of

the tripole. Some stability features are addressed in §5, and §6 concludes with a summary of the major results presented in this study.

2. Description of laboratory experiments

2.1. *Experimental arrangement*

The experiments were carried out in a large transparent tank (92.5 cm in diameter, with a maximal working depth of 30 cm), placed concentrically on a turntable whose angular speed Ω was continuously adjustable in the range 0–10 r.p.m. The tank was filled with a layer of homogeneous fluid (ordinary tap water) with a kinematic viscosity ν and layer depth H. In the majority of the experiments the fluid had a free surface, which was assumed to be free of any stresses. After the table was set in motion, the fluid was allowed to spin-up until a state of solid-body rotation was reached. In the majority of the experiments to be discussed below, the experimental parameters had the following values: $\Omega \approx 0.5$–1.0 rad/s and $H \approx 15$–20 cm. With a water temperature of typically 10–15 °C, the spin-up thus usually took about 40–50 revolutions of the turntable. Both cyclonic and anticyclonic vortices were created by briefly stirring the fluid inside a thin-walled, circular, bottomless cylinder that was placed at the centre of the rotating tank. After allowing the fluid to reach a state of almost purely horizontal swirling motion, the cylinder was swiftly lifted vertically, thus releasing the vortex in the solidly rotating ambient fluid. The subsequent vortex motion was visualized by addition of dye to the fluid in the central cylinder before lifting it, and the evolving flow was recorded photographically by a remote-controlled corotating camera mounted some distance above the free fluid surface. Quantitative information about the relative flow field was obtained by streak photography of small tracer particles floating on the free surface. The information thus obtained for the surface flows is representative of the fluid motion at lower levels, because at all stages after the vortex release the flow is observed to be essentially two-dimensional – an effect caused by the basic rotation of the fluid system.

In some additional experiments (see Kloosterziel & van Heijst 1991) vortices were generated in an alternative way, viz. by the so-called 'collapse technique' which basically consists of the fluid level inside the inner cylinder being different from the outer fluid level. For example, in the case of the inner level lower than outside, the gravitational collapse occurring immediately after lifting of the cylinder results in a flow directed radially towards the rotation axis. Within typically one rotation period, however, this radial flow is deflected until a dynamically adjusted state of cyclonic swirling flow is reached, as can be understood from conservation of angular momentum. As in the case of a stirring-induced vortex, the flow in this adjusted state is governed by a balance between the Coriolis force, the centrifugal force and the pressure gradient force, a balance that is usually referred to as 'gradient flow' (see Holton 1979). The vortices thus created are usually characterized by a radial vorticity distribution that is different from the vorticity profile associated with the stirring-induced vortices, and this may under certain circumstances lead to a different stability behaviour as is discussed in more detail by Kloosterziel & van Heijst (1991*a*). The present paper focuses on vortices created by the stirring technique.

2.2. *Observations*

It was found in the laboratory experiments that the stirring-induced vortices eventually became unstable in all cases. As described by Kloosterziel & van Heijst (1989, 1991*a*), however, the cyclonic and anticyclonic vortices show a dramatically different instability behaviour: the anticyclonic stirring-induced vortex usually splits up into two dipoles moving in opposite directions away from the original vortex centre, whereas its cyclonic counterpart shows a transformation into a compact tripolar vortex. The emergence of such a cyclonic tripolar vortex in the laboratory was first reported by van Heijst & Kloosterziel (1989) and by Kloosterziel & van Heijst (1989). The tripole consists of an elongated cyclonic central vortex with two anticyclonic satellite vortices at its longer sides; in addition, the axis of this tripolar vortex configuration is observed to rotate cyclonically. The formation of a tripole from an initially circularly symmetric vortex can be clearly seen on the plan-view photographs in figure 1 (plate 1). In this experiment the stirred fluid initially confined in the bottomless cylinder was coloured by addition of fluorescent dye. The first photograph (*a*) was taken shortly after the vortex was released in the solidly rotating ambient fluid by lifting this inner cylinder. In this stage shear-induced turbulent motion – or sometimes even overturning motions due to centrifugal instabilities if the Rossby number is very large (see Kloosterziel & van Heijst 1991*a*) – occurred at the circumference of the vortex, as can be seen from the irregular edge of the green dye patch. In the next stage, however, this small-scale motion vanishes and a regular smooth two-dimensional vortex flow is established (see figure 1*b*). The irregularities at the edge of the dyed region are seen to get smeared out by the shear flow at the vortex edge. Although this 'smoothed' vortex is initially circularly symmetric, it soon loses this symmetry, as can be seen in figure 1(*c*). This asymmetry soon becomes more pronounced (figure 1*d*), and two anticyclonic satellite vortices are observed to arise along the longer sides of the now elliptical central vortex: the tripolar vortex is formed (figure 1*e*, *f*). The axis of the tripole rotates steadily about the centre of the core vortex, as can be seen by comparing the orientations of the tripole in the last two frames of figure 1. This rotation of the tripole is cyclonic. Once formed, the structure of the vortex does not change appreciably during a relatively long period of time. The Ekman layer at the tank bottom causes the vortex to spin-down, of course, and this effect is observed in the gradual slow-down of the flow and the decreasing angular speed of the tripole rotation. Viscous effects also induce changes in the vorticity distribution, but at all times the tripole structure persists. This scenario in fact could serve as a definition of a stable tripole. As will be discussed in §5, depending on the precise initial conditions, unstable tripoles may form, which split up into two dipoles.

In order to obtain quantitative information about the flow field, experiments were carried out in which the flow was visualized by small tracer particles floating on the free surface. For the purpose of contrast enhancement, the fluid was dyed with methylen blue such that the white particles show up as bright spots. Figure 2 shows a sequence of streakline photographs taken at subsequent times during the transition from a circular, monopolar vortex to a stable, tripolar flow structure. As can be seen in figure 2(*a*), the initial cyclonic vortex has circular streamlines, but very soon it becomes slightly elliptical, while two weak anticyclonic satellite vortices develop at its sides (figure 2*b*, *c*). Gradually, these satellites become more pronounced (figure 2*d*, *e*), finally resulting in a well-developed tripole vortex (figure 2*f*). As in figure 1, the rotation of the tripole is evident from a comparison of the alignment of the three

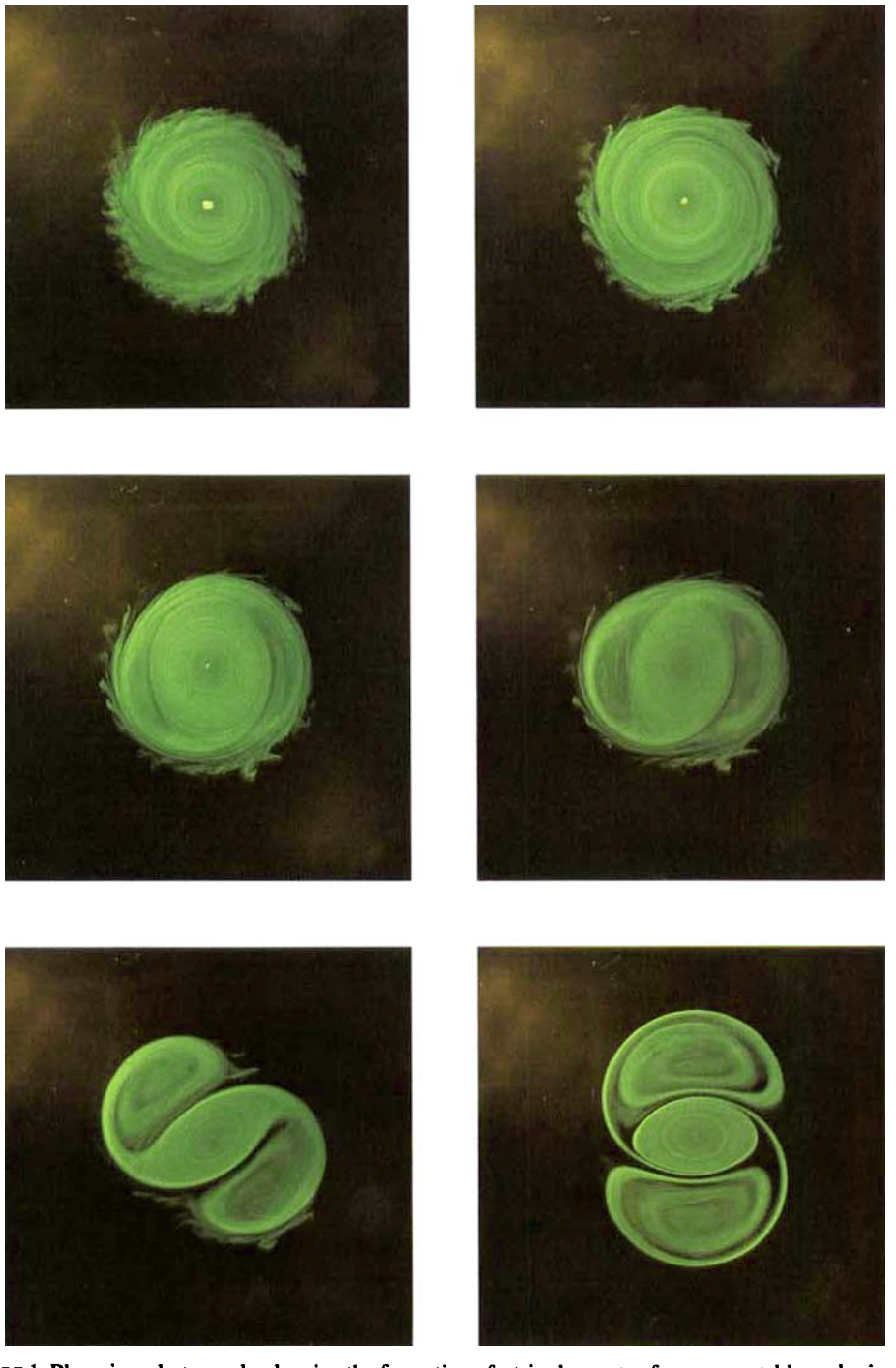

FIGURE 1. Plan-view photographs showing the formation of a tripolar vortex from an unstable cyclonic vortex produced by the 'stirring technique' (see text). The stirred fluid initially confined in the inner cylinder was dyed by addition of fluorescein. The photographs were taken at times (*a*) $t = 1.25T$, (*b*) $2.34T$, (*c*) $4.2T$, (*d*) $5.2T$, (*e*) $5.9T$ and (*f*) $7.0T$ after withdrawing the inner cylinder, with T=6.4 s the rotation period of the turntable. Experimental parameters: $\Omega = 0.98$ rad/s, $H = 18.2$ cm, diameter of inner cylinder $2R_0 = 20.0$ cm.

(Facing p. 304*)*

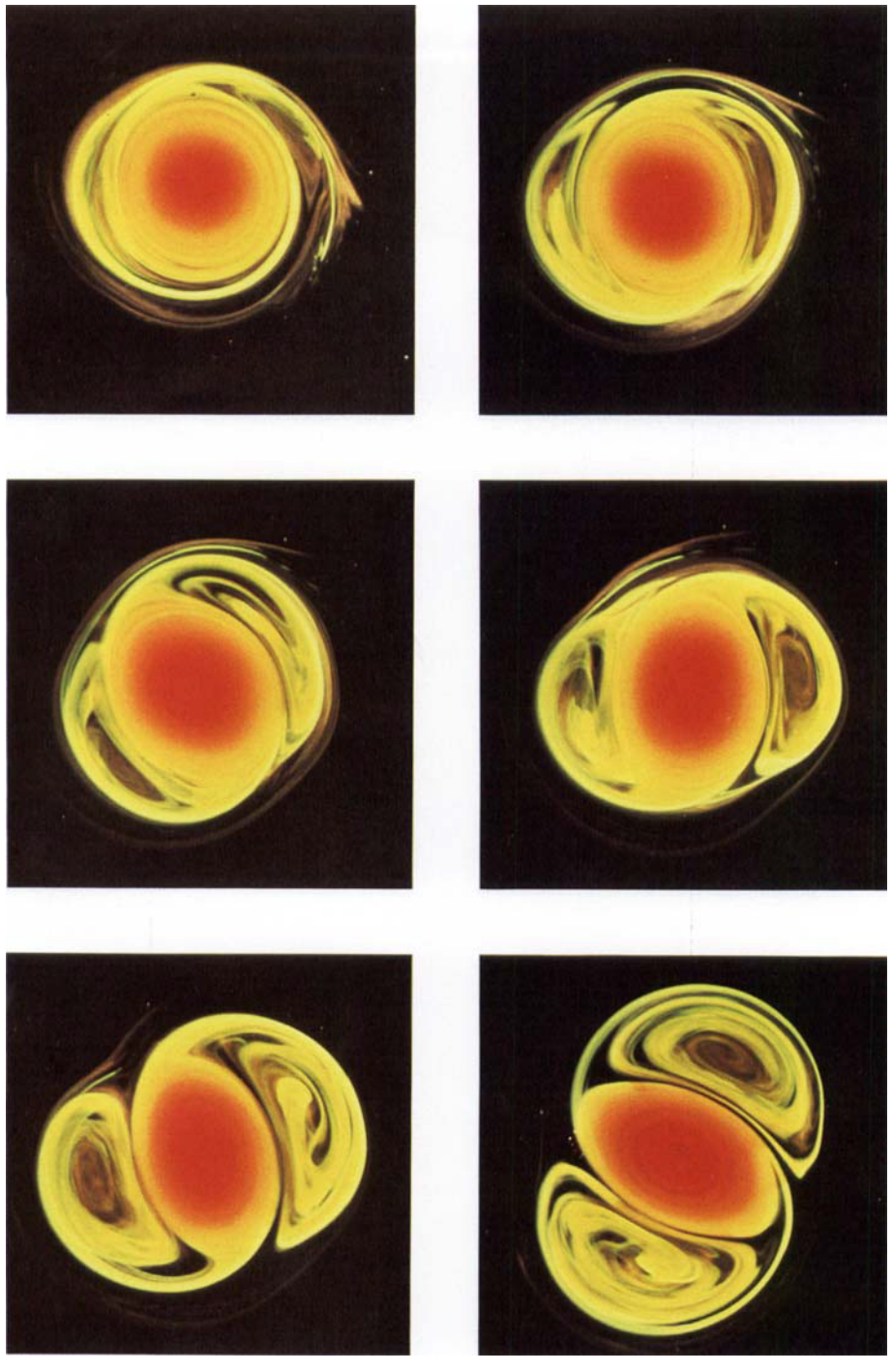

FIGURE 3. Plan-view photographs taken during the formation of a tripole from an unstable, initially monopolar cyclonic vortex. The experiment is essentially similar to the one shown in figure 1, but now the initial vortex is coloured with two different dyes: the core with Terasil Rot G, and the outer ring with fluorescein (yellow/green). The sequence clearly illustrates that the satellites of the tripole consist of yellow-coloured fluid, i.e. of fluid initially confined to the outer ring of the monopolar vortex. The photographs were taken at (*a*) $t = 3.9T$, (*b*) $5.9T$, (*c*) $7.5T$, (*d*) $8.4T$, (*e*) $10.3T$ and (*f*) $12.8T$ with $T = 6.4$ s the rotation period of the turntable. Experimental parameters: $\bar{H} = 18$ cm, $\Omega = 0.98$ rad/s, $2R_0 = 11$ cm.

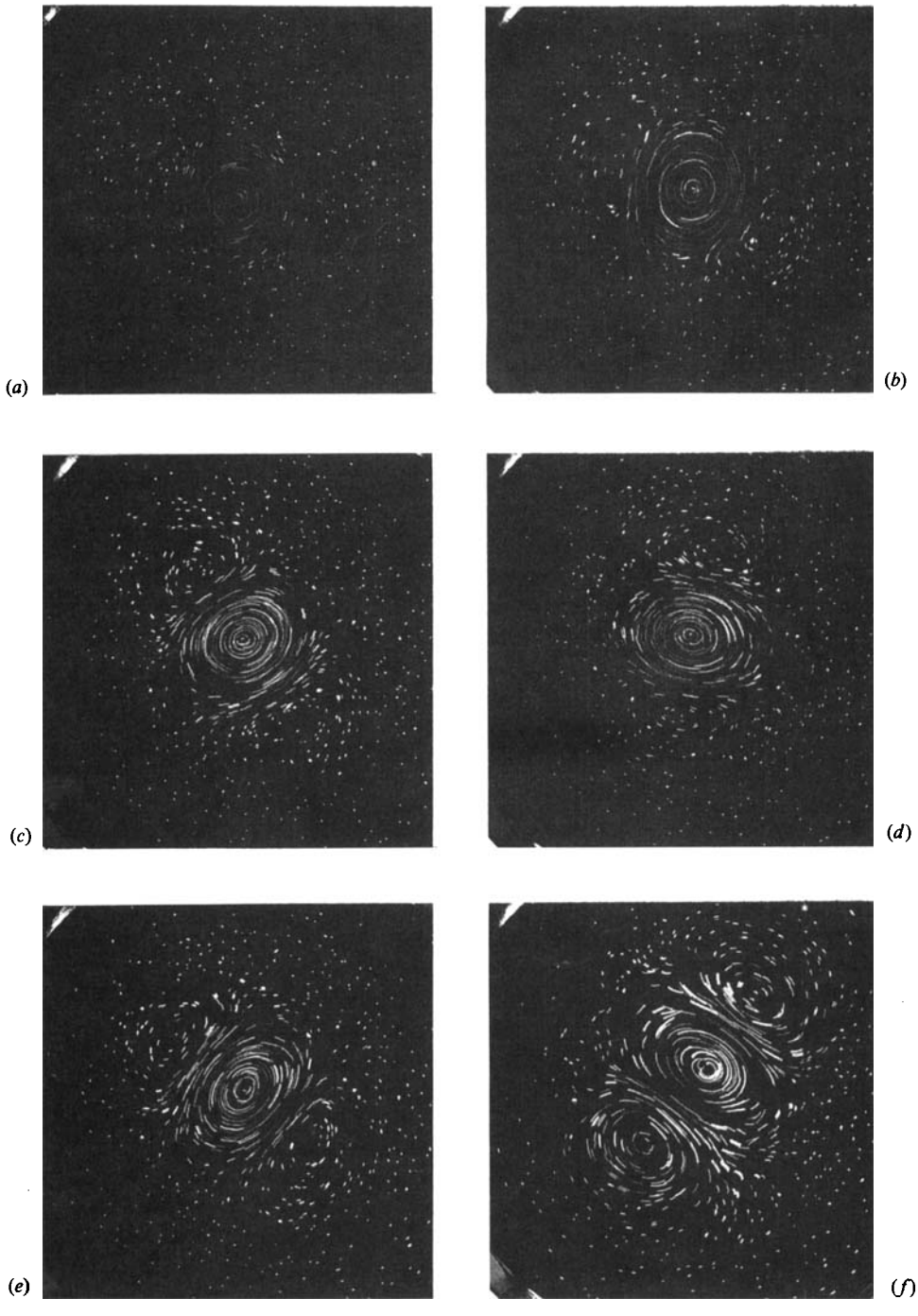

FIGURE 2. A sequence of plan-view streakline photographs illustrating the formation of a tripolar vortex from an unstable cyclonic vortex. This initial monopolar vortex was created by locally stirring the fluid, without any confinement by an inner cylinder. The flow was visualized by small tracer particles floating on the free surface. The photographs were taken at (*a*) $t = 0.0T$, (*b*) $3.1T$, (*c*) $4.7T$, (*d*) $6.3T$, (*e*) $7.0T$ and (*f*) $12.5T$, with $T = 6.4$ s the rotation period of the turntable; the exposure times were (*a*) 0.5 s, (*b–e*) 1.0 s and (*f*) 2.0 s. Additional experimental parameters: $\Omega = 0.98$ rad/s, $\bar{H} = 18.0$ cm.

vortices on the consecutive photographs. By measuring the streak lengths, this visualization technique allows one to monitor the evolution of the velocity field and also to calculate the spatial distribution of the vorticity and other important flow parameters; this will be discussed in the next section.

In comparison with streak photography, flow visualization by adding dye has an important advantage in that it provides information about the redistribution of material elements during the evolution of the initial monopolar vortex to the ultimate tripole structure. In order to examine the formation of the satellite vortices, a few experiments were carried out in which the initial vortex was coloured with two different dyes. A typical result of such an experiment is shown in figure 3 (plate 2). As can be seen in figure 3(*a*), the core of the initial vortex was coloured red (with Terasil Rot G), while the outer ring was dyed yellow/green with fluorescein. In the next two frames (figure 3*b*, *c*) the core of the vortex is observed to become increasingly elliptical, without any appreciable form changes in the yellow outer ring. In the next stage the tripole formation becomes evident, and the yellow fluid surrounding the core of the vortex is seen to get concentrated in the two satellites (figure 3*d*, *e*). The ultimate tripole consists of a red-coloured cyclonic core vortex flanked by two yellow/green-coloured satellite vortices (figure 3*f*).

In §3 of this paper the details of tripole formation will be considered in terms of the spatial distribution of the vorticity, and it will be shown that the initial cyclonic vortex consists of a core of positive relative vorticity enclosed by a ring of negative relative vorticity, whereas in the tripole the negative vorticity is completely confined to the two satellite vortices alongside the central cyclonic vortex. In other words, the yellow and red dyes in the experiment of figure 3 can be thought of as being representative of anticyclonic and cyclonic vorticity, respectively, and the changing colour patterns nicely illustrate the redistribution of vorticity throughout the tripole formation.

3. Measurements of the flow characteristics

Along with experiments in which the phenomenon of the tripole formation was merely visualized, additional experiments were carried out in order to measure the actual flow field during the various stages of the tripole formation and the subsequent decay process. In this section the quantitative reconstruction of the flow field from the streakline photographs by digitization of the streaks will be described. The information thus obtained enables one to calculate the associated flow properties such as the distribution of vorticity and the corresponding stream function, which are essential ingredients needed for a clear picture of the tripole formation, stability properties and the decay process. The mature, stable cyclonic-core tripole is characterized by a cyclonic rotation of its axis, and measurements of the rotation speed will be described below. The decay of the tripole is monitored in terms of the decreasing vorticity maximum in the core vortex as well as in terms of the circulations of the three vortical regions. Several other quantitative observations will be discussed too, thus providing an overview of the properties of laboratory tripoles.

3.1. *Digitization of the flow field*

Quantitative information about the evolving flow field was obtained from streakline photographs such as the ones shown in figure 2. For a number of particle paths the streak lengths were measured from an enlarged projection of the photograph, by digitizing the end points of the streaks. This digitization was carried out by hand on

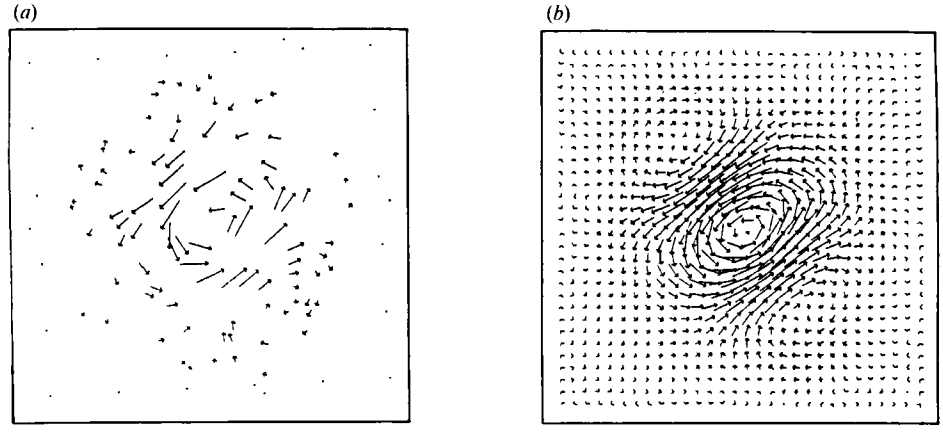

FIGURE 4. A characteristic example of the digitized flow field. The vector field shown in (*a*) is obtained from a streakline photograph, by measuring streak lengths and dividing by the exposure time. For the case of a 30×30 grid, the interpolated velocity field is shown in (*b*). The vortex was created by cyclonically stirring in an unconfined region in the rotating tank. The digitized photograph was taken at $t = 9.4T$ after the forcing was stopped, with $T = 6.4$ s the rotation period of the turntable. The average water depth was $H = 15$ cm.

an electronic digitizing pad connected to a personal computer. The length of each streak is then divided by the exposure time, thus yielding the average local velocity vector. An example of the digitized velocity field is presented in figure 4(*a*); the tripolar structure is clearly discernable. Subsequently, the velocity field $\boldsymbol{v}$ is calculated on a rectangular grid by numerical interpolation using an algorithm described to some detail by Nguyen Duc & Sommeria (1988). For the case of a 30×30 grid the interpolated velocity field is shown in figure 4(*b*), in which the tripole structure is easily recognized. For a 'smooth' interpolation the digitized flow field should have a homogeneous spatial distribution of vectors; one should therefore avoid any clustering of vectors, because this may locally lead to unphysically large gradients in the vorticity of the interpolated field. For this reason, vectors are omitted in areas where many are too close together.

Once this interpolated flow field is determined, it is possible to derive some more specific information about the tripole structure, such as the velocity distribution along any particular cross-section through the tripole. For this purpose a routine was developed for plotting the velocity components perpendicular and parallel to some prescribed straight line through a particular region of interest. If the grid is sufficiently fine, a good approximation is found by simply decomposing the velocity vectors on the interpolation grid that are within some prescribed distance δ from the cross-sectional line into normal and tangential components. This approximative technique was the basis for that routine, and some examples of velocity distributions along a few interesting cross-sections through the tripolar vortex are given in figure 5. It should be kept in mind that these velocities were measured in the reference frame of the rotating tank. The velocity relative to the rotating tripole structure can be obtained by correcting for its rotation, but because of the small value of the rotation speed this would hardly affect the velocity distribution as presented in figure 5.

One of the other relevant quantities that can be derived from the interpolated velocity field is the vorticity $\boldsymbol{\omega} \equiv \boldsymbol{\nabla} \wedge \boldsymbol{v}$. Assuming the flow to be quasi-two-dimensional and close to divergenceless (this is certainly the case for rapidly rotating

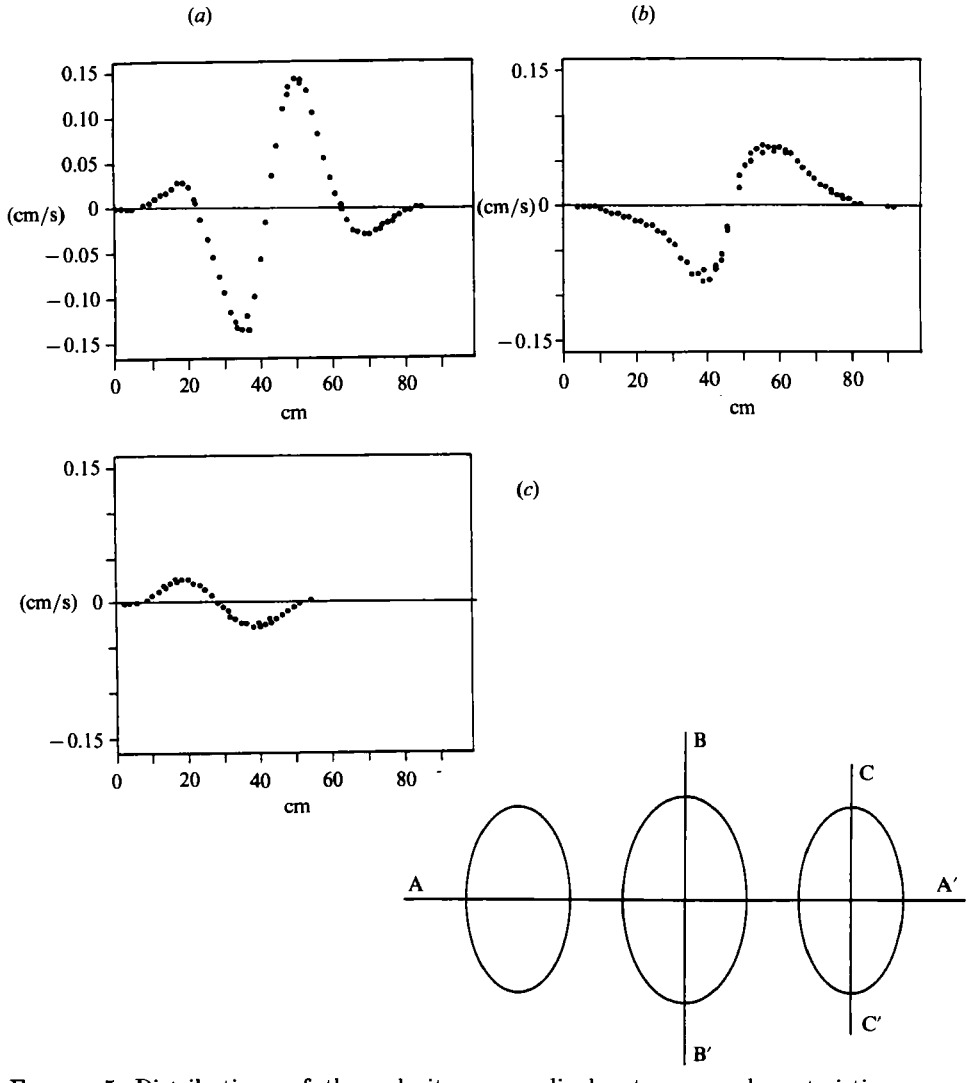

FIGURE 5. Distributions of the velocity perpendicular to some characteristic cross-sections through the tripole vortex shown in figure 4: (*a*) the major tripole axis AA′, (*b*) the minor axis BB′, and (*c*) a cross-section through one of the satellites CC′. The data points in the graphs are obtained from the interpolated velocity field. The Rossby number of the tripole, based upon the maximum relative velocity and its distance to the vortex centre, is approximately 2.

systems with reasonably small Rossby numbers), a stream function ψ may be introduced, defined indirectly by $\boldsymbol{v} = \boldsymbol{\nabla} \wedge \boldsymbol{k}\psi$, with $\boldsymbol{k}$ the unit vector in vertical direction and $\boldsymbol{v} = (u, v)$ the planar velocity field with components u and v (here referred to in rectangular coordinates (x, y)). It is obvious that the vorticity $\boldsymbol{\omega}$ has a vertical component ω_z only. The scalar vorticity can be determined on each grid point by differentiation of the velocity field, according to

$$\omega_z = \frac{\partial v}{\partial x} - \frac{\partial u}{\partial y}. \tag{1}$$

Nguyen Duc & Sommeria (1988) estimated the relative error in the vorticity derived in this manner from the interpolated flow field to be approximately 10%.

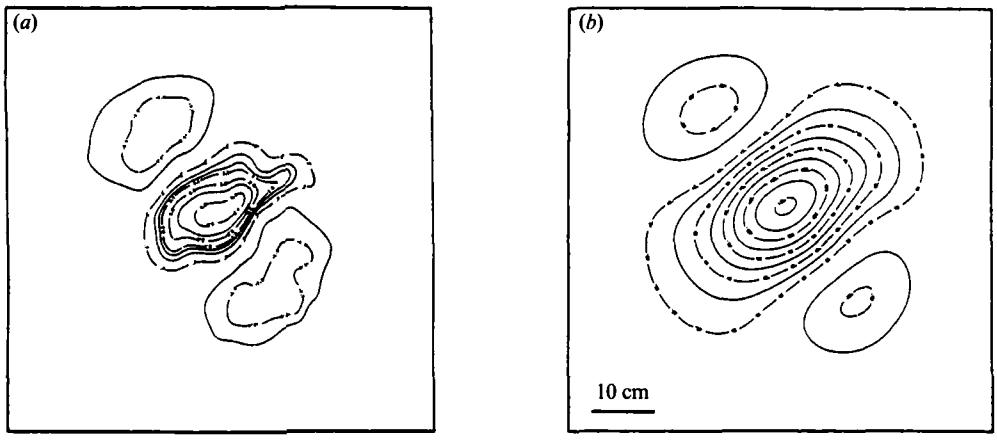

FIGURE 6. Isoline plots of (*a*) the vorticity and (*b*) the stream function as calculated from the interpolated velocity field shown in figure 4(*b*).

The stream function was in turn determined by numerically solving the Poisson equation

$$\nabla^2\psi = -\omega, \tag{2}$$

where ∇^2 is the Laplace operator (the subscript z is from here on dropped from the vorticity). On the boundary of the rectangular domain of integration, the stream function is taken to be constant. A graphical representation of some isolines of ω and ψ associated with the velocity field shown in figure 4 is given in figure 6. Both isoline patterns show the tripole structure of the flow. In most of the graphs the isovorticity contours may locally be a little erratic, whereas the streamlines show a much smoother pattern: the irregularities in the vorticity pattern are 'ironed out' by the integration of (2).

A major general conclusion that can be drawn from the vorticity contour plot (which is representative of 'mature' tripoles as monitored in other experiments) is that the anticyclonic vorticity is entirely concentrated within the two satellite vortices, and likewise the cyclonic vorticity in the central vortex. In each of the three regions visible in figure 6(*a*) the vorticity is continuously distributed. This vorticity pattern is typical for a tripole in the earlier stages after its formation, with the anticyclonic vortical regions close to the core and rather elongated: the tripole then essentially consists of one compact structure with distributed vorticity of both signs.

3.2. *Tripole formation process*

In general, one observes an evolution of the vorticity field that is schematically indicated in figure 7. Initially, a monopolar vortex, as mentioned before, consists of a core of positive relative vorticity (the hatched region in figure 7*a*) that is surrounded by a ring of negative vorticity (the non-hatched region in figure 7*a*). After a transition period, initiated by the growth of a wavenumber 2 perturbation, the flow equilibrates in the 'tripolar state' which is sketched in figure 7(*c*). During the transition period the topological character of the vorticity field appears to change drastically. Whereas, initially, the region of negative vorticity consists of one set of nested contour levels, after equilibrium is reached, the negative vorticity is found in two disconnected sets of nested contour levels. It will be clear that no continuous map $f: \mathbb{R}^2 \to \mathbb{R}^2$ exists that can map the vorticity distribution of figure 7(*a*) to that

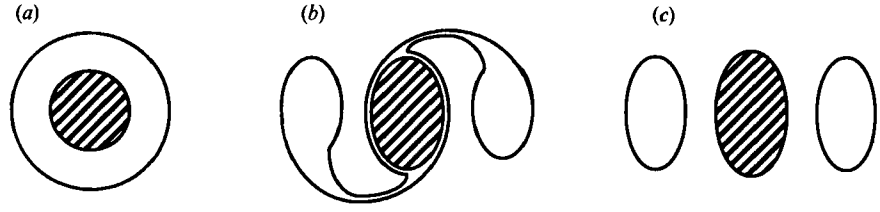

FIGURE 7. Diagram illustrating the change of the vorticity distribution during the evolution of an isolated monopole which is schematically indicated in (*a*) as a ring of positive vorticity (hatched region) surrounded by a ring of negative vorticity (non-hatched region). A flow that conserves vorticity can take the configuration shown in (*a*) to that shown in (*b*) but not to (*c*).

shown in figure 7(*c*). Smooth maps do exist though, which map the initial configuration onto that of figure 7(*b*). If, as a working hypothesis, one assumes that the flow is two-dimensional, inviscid and incompressible, then such a map is provided for by the flow itself. Considering time as a parameter, the one-parameter map induced by the flow is $g_t: \mathbb{R}^2 \to \mathbb{R}^2$ with $g_t \boldsymbol{x}(0) = \boldsymbol{x}(t)$, where $\boldsymbol{x}$ is the position of a fluid element at time t. Ideal planar, incompressible flows can take the vorticity from the configuration of figure 7(*a*) to that of figure 7(*b*) but not to that of figure 7(*c*), as a consequence of Kelvin's circulation theorem, i.e. the conservation of vorticity: $\mathrm{D}\omega/\mathrm{D}t = 0$. By dyeing a fluid element one can trace the motion of that element, and the photographs of figures 1 and 3 show that during the evolution, the whole vortex is deformed and torn out, but at all times remains connected. The fact that the negative vorticity becomes ultimately concentrated in two distinct and disconnected regions thus seems to be a viscous effect: the considerable shear one would find in the thin filaments connecting the satellites with the core (see figure 7*b*), is dissipated by the slightest amount of viscosity. These filaments remain visible in the dye structure, since the diffusion of dye is not related to the diffusion of momentum.

The tripole formation is intimately linked to the structure of the initially circularly symmetric vortex. It is hard to generate cyclones in the rotating tank which do stay circularly symmetric and show no transition into a tripolar flow structure (for example, the 'sink' vortices discussed by Kloosterziel & van Heijst (1991*b*) appear to be quite stable). In the realm of purely two-dimensional (planar) incompressible, inviscid flow, Rayleigh's inflexion-point theorem states that a necessary condition for instability in the linearized evolution is that the gradient of the vorticity changes sign at least once (see Drazin & Reid 1981). The growing disturbances associated with such an instability are non-axisymmetric and lead to a destruction of the initial circular symmetry of the streamline and vorticity patterns. Typically, the cyclonic stirring vortices studied in this paper are isolated, i.e. have vanishing circulation for larger radii, and generally consist of a core of positive relative vorticity, surrounded by a ring – of finite width – of negative vorticity. Observations reveal that the radial distribution of azimuthal (swirl) velocity in a vortex prior to transforming into a tripole can often be closely approximated by a simple Gaussian function; an example of such a velocity distribution is presented in figure 8. The solid line is a fit to the data with a curve

$$v(R) = \tfrac{1}{2} U R \, \mathrm{e}^{-\frac{1}{2}R^2}, \tag{3}$$

where U is an appropriate velocity amplitude and R the non-dimensionalized radius $R \equiv r/L$, with L a lengthscale chosen such as to have the maximum of v coincide with

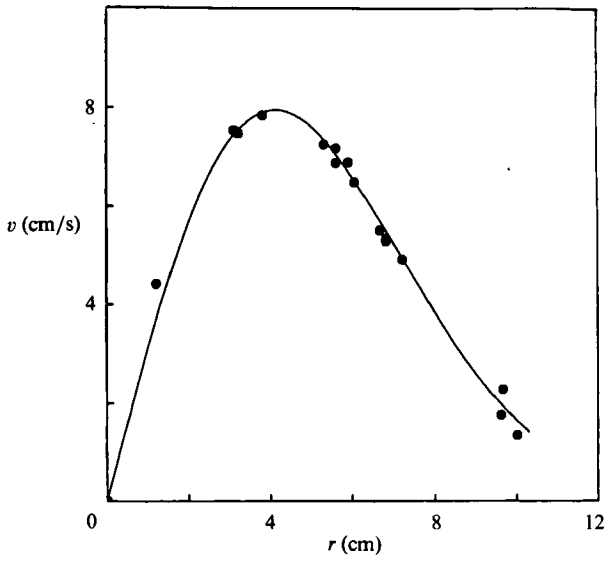

FIGURE 8. Azimuthal velocity distribution of a cyclonic, stirring-induced barotropic vortex prior to transforming into a tripole. Experimental data are denoted by black dots while the solid line represents the fitted curve given by (3).

that of the observed distribution. The corresponding stream function is (dimensionally)

$$\psi(R) = \tfrac{1}{2}UL\,\mathrm{e}^{-\frac{1}{2}R^2} \tag{4}$$

and the vorticity

$$\omega(R) = \frac{U}{L}(1-\tfrac{1}{2}R^2)\,\mathrm{e}^{-\frac{1}{2}R^2}. \tag{5}$$

The gradient of this vorticity distribution, representative of typical conditions leading to tripole formation in the laboratory, is

$$\frac{\mathrm{d}\omega}{\mathrm{d}R} = \frac{U}{L^2}(\tfrac{1}{2}R^3-2R)\,\mathrm{e}^{-\frac{1}{2}R^2}$$

and obviously changes sign at a non-dimensional radius $R = 2$. This particular profile satisfies Rayleigh's inflexion-point theorem, and instabilities can therefore in principle set in (but not necessarily). Numerical experiments of Carton *et al.* (1989) indeed show tripole formation in simulations of the fully nonlinear evolution (with added hyperviscosity) of Gaussian vortices perturbed with wavenumber-2 disturbances.

One may argue that the laboratory flow is not two-dimensional; first of all because there is a spatially varying fluid layer depth and secondly because vertical velocities are not ruled out during the evolution of the vortex. In rapidly rotating systems, for small-Rossby-number flows, the vertical velocities possibly involved in certain instability mechanisms, are expected to be small, though. The free-surface deformability – with the associated possibility of vorticity generation by vortex stretching – is of no importance in the tripole formation, as simple experiments show: tripole formation is not suppressed by covering the tank with a rigid cover. This observation also shows that the formation of tripoles is not related to a kind of topographic forcing by the parabolic free surface. In fact, tripole formation has also been observed to take place over strongly sloping bottom topography and away from

the tank centre (see Carnevale, Kloosterziel & van Heijst 1991). Still, however, there remains the possibility that vertical velocities are involved in the instability mechanism. Consider for instance the rigid-lid case, with the boundary conditions that the vertical velocity is zero both at the bottom and the upper (rigid) surface. If a circularly symmetric vortex is imagined to be exactly centred in the rotating tank, then the results stated by Chandrasekhar (1961) can straightforwardly be generalized. A normal-modes analysis of the linearized set of equations for the complete three-dimensional problem shows that the onset of instability is determined (in the linear context) by the sign of the so-called Rayleigh discriminant $\Phi(r)$ that can be defined as

$$\Phi(r) = \frac{\mathrm{d}}{\mathrm{d}r}(vr)^2, \tag{6}$$

where v is the azimuthal velocity. The results are that the flow is stable to axisymmetric disturbances whenever the discriminant is positive everywhere, whereas it is unstable if it is negative somewhere (this is a sufficient condition for instability). For non-axisymmetric disturbances the flow is unstable too if the discriminant is negative but positiveness cannot be shown to ensure instability or stability. In both cases, that is, axisymmetric and non-axisymmetric, vertical velocities necessarily occur.

By replacing v in the expression for the discriminant by $v+\Omega r$, with Ω the rotation rate of the tank, the equivalent necessary and sufficient condition for instability of a vortex in the centre of the tank is that the non-dimensional product $(\epsilon\tilde{v}+R)\,(\epsilon\tilde{\omega}+2)$ is negative somewhere. In the above expression $\tilde{v} \equiv v/U$, $\tilde{\omega} \equiv \omega/(U/L)$ and ϵ is the Rossby number: $\epsilon \equiv U/(\Omega L)$. The same expression can also be shown to be valid on an f-plane (with $\Omega = \frac{1}{2}f$). It is not hard to verify that in the case of the above-mentioned Gaussian distribution, representative of cyclones that become unstable and become tripoles, the sign of the product of velocity and vorticity is negative for large enough Rossby numbers, namely, for approximately $\epsilon > 4.5$. For anticyclones the Rossby number merely needs to exceed a value of about 0.65. In view of Chandrasekhar's results, it can be concluded that if the Rossby number of a cyclonic vortex exceeds this rather high value of 4.5, centrifugal instabilities will emerge in the form of axisymmetric and non-axisymmetric overturning motions, although *a priori* it is not clear which mode has the largest growth rate. For smaller Rossby numbers (in the linear evolution) axisymmetric disturbances will not amplify but growing non-axisymmetric disturbances are not excluded. It remains a matter of speculation, therefore, whether the observed evolution is governed mainly by two-dimensional dynamics or whether three-dimensional effects do play a role after all. The explosive instability of most anticyclonic vortices – as compared to their cyclonic counterparts – (see Kloosterziel & van Heijst 1989) indicates that three-dimensional effects can be important (in purely two-dimensional flows there is no difference in stability between cyclones and anticyclones). The free surface itself does not seem to play an active role and can be excluded from most considerations. The striking resemblance between the evolution in the laboratory and the numerical two-dimensional simulations of Carton *et al.* (1989), and the observation that during the evolution all motion appears to take place in Taylor columns, indicates that the tripole evolution is close to two-dimensional.

3.3. *The tripole rotation*

As remarked in §2, a characteristic feature of a laboratory tripole is that it rotates around a vertical axis through the centre of the core vortex, relative to the frame of

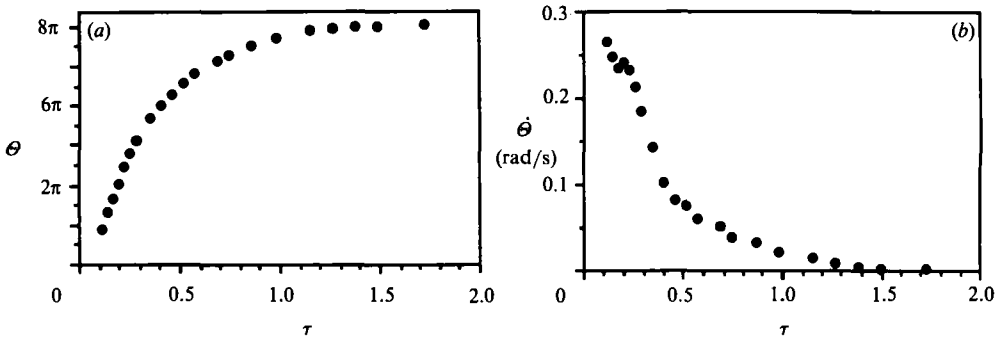

FIGURE 9. The rotation speed of the tripole is determined by measuring its orientation angle Θ relative to the rotating frame at subsequent times during the experiment. A typical result of such measurements is shown in (a), and differentiation with respect to time yields the rotation speed $\dot{\Theta}$ as represented graphically in (b). In both graphs the data have been plotted versus the non-dimensional time $\tau \equiv t/T_{\mathrm{E}}$, where T_{E} is the Ekman timescale defined by (7). Experimental parameters: see figure 2.

reference of the rotating system. For a number of experiments the orientation angle Θ relative to some arbitrary initial orientation was measured from sequences of photographs taken during an experiment. A typical result is shown in figure 9(a) where the angle Θ is plotted as a function of the dimensionless time $\tau \equiv t/T_{\mathrm{E}}$, with T_{E} the Ekman timescale defined as

$$T_{\mathrm{E}} \equiv \frac{\bar{H}}{(\nu\Omega)^{\frac{1}{2}}}, \tag{7}$$

where $\bar{H}$ is the average fluid depth and ν the kinematic viscosity. Although it is not clear *a priori* that the Ekman timescale is the relevant one for the decaying tripole, it is clear from figure 9(a) that – at least for the rotation – it seems the right choice (note that the tripole has come to a virtual standstill after a period equal to approximately twice the Ekman time). The data shown in figure 9(a) suggest an exponential slow-down of the rotation rate, i.e.

$$\dot{\Theta}(\tau) = \dot{\Theta}(0)\,\mathrm{e}^{-\alpha\tau}, \tag{8}$$

where a dot denotes differentiation with respect to τ. The angular speed $\dot{\Theta}$ corresponding to the observations shown in figure 9(a), is shown in figure 9(b). Essentially the same data set is shown in figure 10, but now the angular speed $\dot{\Theta}$ is normalized by its value at $\tau = 0$ and plotted logarithmically versus the dimensionless time. The straight line through the data shows that the decay is indeed close to exponential, that is, according to (8). The slope of the line in figure 10 (which has been fitted by eye) is approximately $\alpha = 3.1$. In other experiments a similar exponential decrease of the rotation speed was found, but with different values of α, namely ranging from 1.9 to 3.9. Although the reason for these differences are at this stage unclear, it is felt that the variations in the observed α-values are somehow related to the properties of the initial vortex (its diameter and Rossby number). As will be discussed hereafter, the tripole decay is a complicated process, being partly caused by the spin-down mechanism associated with the bottom Ekman layer, and partly by the lateral entrainment of ambient fluid.

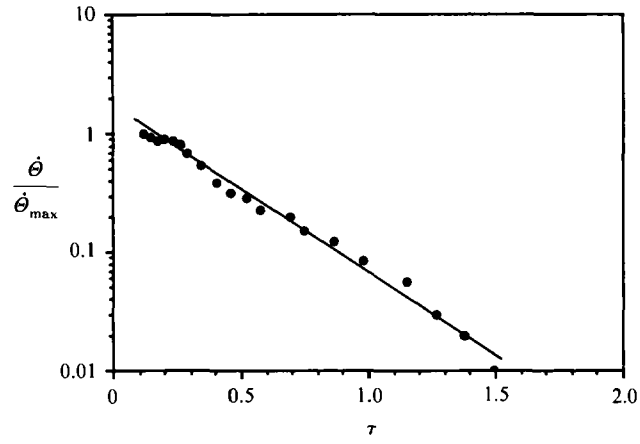

FIGURE 10. The same data of the tripole rotation speed $\dot{\Theta}$ as presented in figure 9, but now normalized by the maximum value $\dot{\Theta}_{max}$ in the data set, and plotted on a logarithmic scale. The straight line has been fitted to the data by eye.

3.4. *Scatter plots*

On typical dynamical timescales that are much smaller than the Ekman time or a simple diffusive timescale (a few eddy turnover times), it appears that the tripole is close to stationary in a frame of reference that is corotating with the tripole. In this frame, to leading order, the Jacobian of the vorticity and stream function vanishes, i.e. $J(\psi', \nabla^2\psi') = 0$, where the primes indicate that the stream function and the vorticity have to be corrected first for the overall rotation of the tripole:

$$\psi' \equiv \psi + \tfrac{1}{2}\dot{\Theta}r^2, \quad \omega' = -\nabla^2\psi' = \omega - 2\dot{\Theta}. \tag{9}$$

Here r measures the distance from the centre of the tripole.

The vanishing Jacobian implies the existence of some functional relation between stream function and vorticity, that is,

$$\nabla^2\psi' = F(\psi'), \tag{10}$$

where F is some function of one variable. This function can be 'measured' by simply plotting the value of vorticity versus that of the stream function as found on each grid point. The result is what is called the 'scatter plot' of the flow. For circularly symmetric vortices the functional relation can be measured directly (i.e. without a rotation correction), and the result for a typical circular vortex just before transforming into a tripole is shown in figure 11. As a matter of fact, this is the scatter plot of the particular vortex that gave rise to the tripole whose digitized properties are shown in figures 4 and 6. Working with a 30×30 grid, some 900 data points have been plotted in figure 11 (*a*). It is seen that the scatter plot defines a function $F(\psi)$ that is close to linear in the positive-vorticity core of the vortex, whereas it is strongly nonlinear in the region of negative vorticity. In this plot each point on the ψ-axis corresponds to a ring of fluid at a certain radius from the centre of the vortex. As remarked in §3.2 and seen in figure 8, these unstable monopoles can often closely be approximated by the Gaussian velocity profile given by (3). Elimination of R between (5) and (4) shows that the function F in this case is

$$\tilde{\omega} = F(\tilde{\psi}) = 2\tilde{\psi}(1 + \log 2\tilde{\psi}), \tag{11}$$

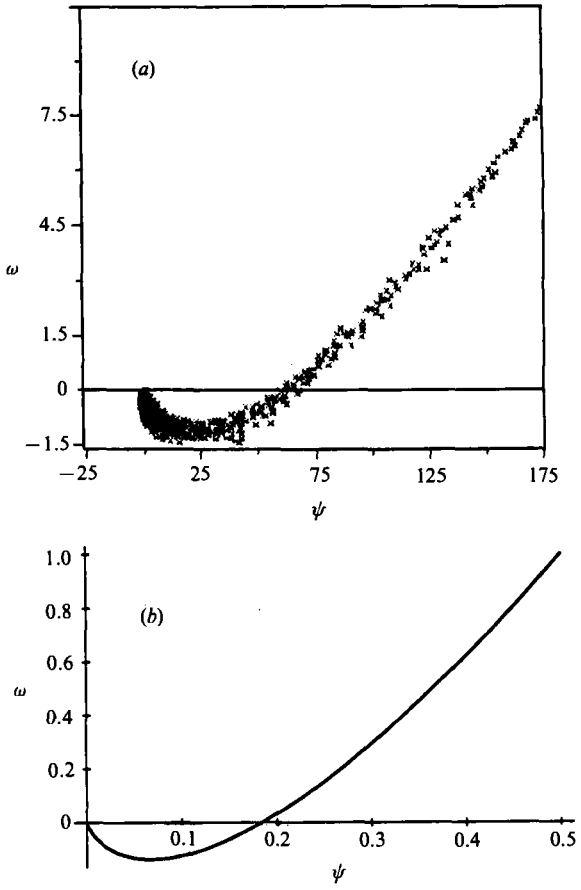

FIGURE 11. Plots showing (*a*) the scatter plot of a cyclonic stirring vortex prior to transforming into a tripole and (*b*) theoretical function relating vorticity to stream function for the Gaussian vortex with a velocity profile given by (3).

where vorticity and stream function have been non-dimensionalized according to $\tilde{\psi} = \psi/(UL)$ and $\tilde{\omega} = \omega/(U/L)$. This function is plotted in figure 11(*b*). Note that $\tilde{\psi}$ runs from $\tilde{\psi} = 0$, which corresponds to the limit $R = \infty$, to $\tilde{\psi} = \frac{1}{2}$, which corresponds to $R = 0$. The resemblance between the curves in figure 11(*a*, *b*) indicates that this particular vortex had to a good approximation a Gaussian structure.

The digitized properties of the tripole emerging from this initially close-to-Gaussian vortex were shown in figures 4 and 6, and its scatter plot is presented in figure 12. The fact that the tripole is not stationary in the original frame of reference, i.e. that of the rotating table, is reflected by the scatter in the lower branch of the (ω, ψ)-plot shown in figure 12(*a*). The scatter indicates that no well-defined relation between vorticity and stream function exists in the satellites (the lower branch has negative vorticity and thus corresponds to the satellite regions), which simply means that in the satellites the vorticity contours do not coincide with the stream function contours. Figure 12(*b*) shows the same scatter plot obtained after correction for the overall rotation of the tripole; it is seen that the lower branch has 'condensed' onto a *well-defined* – almost linear – function, implying that in this frame of reference the isolines do coincide. Note that the upper branch, which corresponds to the region of

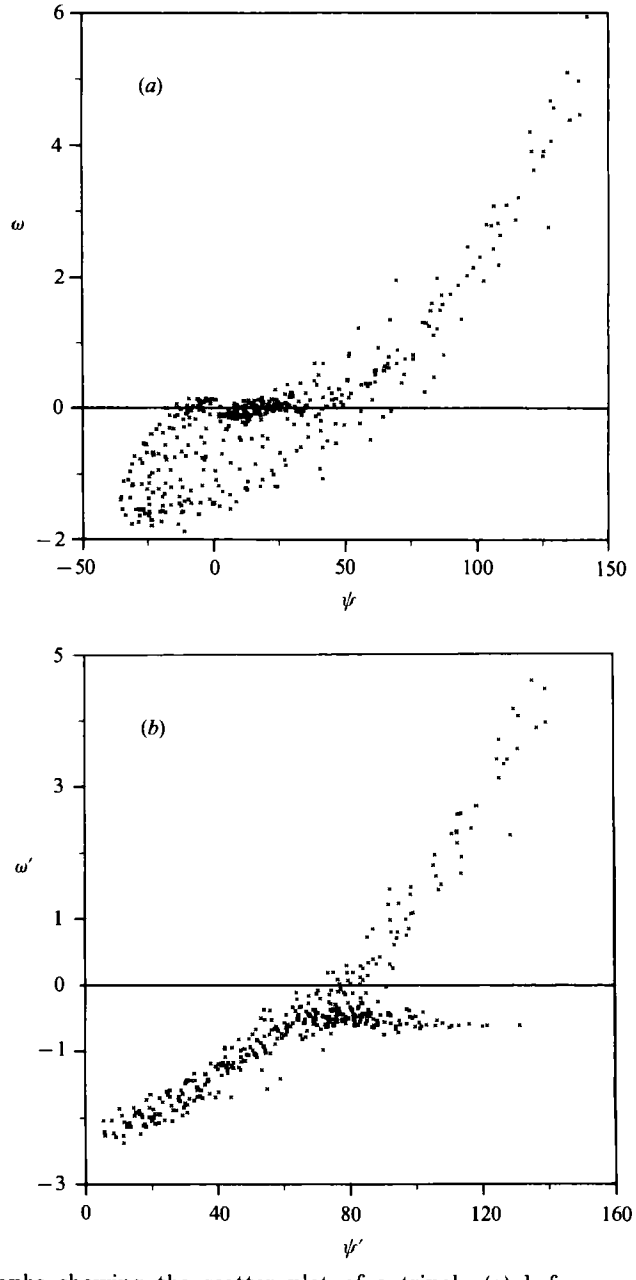

FIGURE 12. Graphs showing the scatter plot of a tripole (*a*) before correction and (*b*) after correction for its rotation. The scatter plots were obtained from the tripole previously shown in figures 4 and 6.

the core of positive vorticity, has not appreciably changed after the correction; this is because in this particular case the vorticity and stream function contours were close to circular in this region and thus hardly affected by an additional rotation. The scatter that remains in figure 12(*b*) is due to small errors, but possibly also reflects the fact that the flow is not exactly stationary.

It may be noted that, compared to the scatter plot of the monopole that became

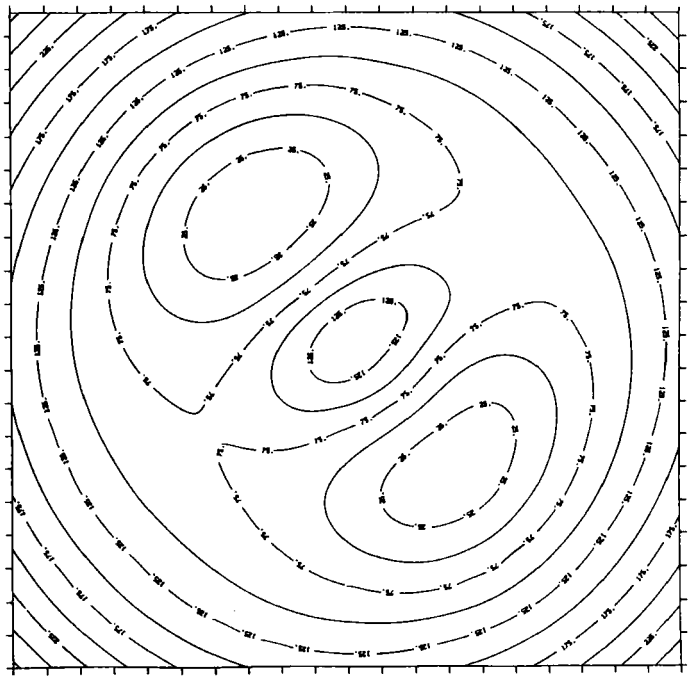

FIGURE 13. Isoline plots of the stream function of the tripole previously shown in figure 6(*b*), but now relative to a frame corotating with the tripole.

unstable (see figure 11), the function relating vorticity to stream function has considerably changed; it now consists of two branches both with a positive slope. Any 'point' on the positive branch of the function indicated by the data in figure 12(*b*) corresponds to a ring of fluid elements in the core of the tripole, whereas any point on the negative branch corresponds to two rings of fluid elements, one in each satellite. The horizontal branch represents the exterior of the tripole, in which the relative flow is irrotational; after the correction for the rotation this region has constant vorticity. The effect of correcting for the tripole rotation can also be seen in figure 13, which presents a contour plot of the stream function relative to a frame corotating with the tripole previously shown in figure 6(*b*). Note the striking resemblance between this relative streamline pattern and the dye pattern as visible on the photograph in figure 1(*f*).

The (ω, ψ) scatter plots are of interest for several reasons. The mere fact than an unstable vortex rapidly equilibrates in the tripole state indicates that this particular ultimate state must be some sort of 'attractor'. (Note that the transition to a tripole occurs on a timescale that is short compared to the viscous timescales.) These attractors for dissipative infinite-dimensional systems are hard to define, but in plasma physics and fluid mechanics some theories have been proposed that tentatively characterize these states as constrained critical points of some suitable variational principle. These theories are based on what is called the 'selective decay hypothesis' for certain dissipative systems (see Hasegawa 1985). In all such theories the predicted state is characterized by some functional relation between the fields of interest; for the 'Taylor minimum-energy state' this is a relation between the magnetic field and its curl (see Taylor 1974) whereas for the so-called 'minimum enstrophy states' of two-dimensional flows it defines a coordinate-free relation

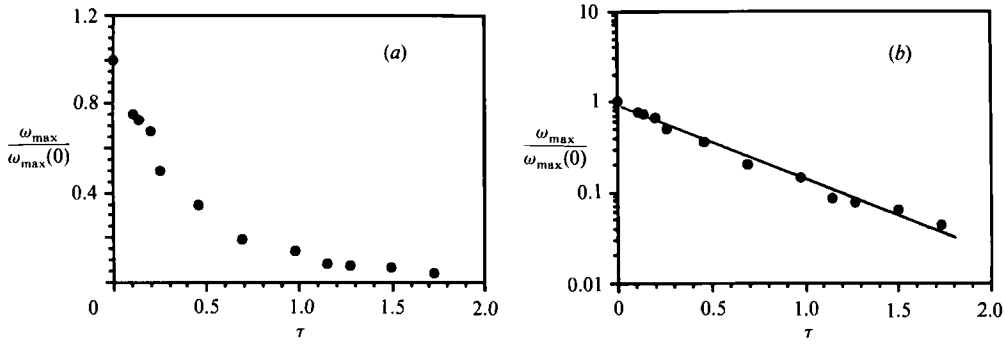

FIGURE 14. Graphical representations of the decreasing vorticity maximum ω_{max} as determined from the digitized flow field. The data are normalized by the initial value $\omega_{max}(0)$ and are plotted in (*a*) as a function of the non-dimensional time τ. Graph (*b*) shows the same data, but now plotted on a logarithmic scale; the straight line has been fitted by eye. Experimental parameters: see figure 2.

between vorticity and stream function (see Leith 1984 and Stern 1975). The scatter plots introduced above can therefore serve as a verification of such proposed theories.

3.5. *Decay*

The slow-down of the tripole rotation speed is directly associated with the decay of the flow within the tripole structure itself. Visual observations revealed that in the final stage, in which the tripole rotation had stopped, the relative flow was virtually zero. In the experiments in which the flow was visualized by addition of dye (like the one illustrated in figures 1 and 3), a well-defined tripolar structure was still clearly visible in the dye distribution, although any relative motions were absent in this ultimate state of rest. This remaining dye pattern ultimately becomes 'blurred', owing to molecular diffusion of the dye. In order to quantify the decay of the tripole vortex, the vorticity maximum – as determined from the digitized flow after interpolation and subsequent differentiation – was plotted as a function of the dimensionless time τ in figure 14(*a*). In this graph the vorticity maximum $\omega_{max}(\tau)$ was normalized by its value $\omega_{max}(0)$ at $\tau = 0$; this starting time $\tau = 0$ corresponds to the time at which the first of the sequence of photographs of the tripole was taken. The gradual decay of the vorticity maximum is obvious, and appears to be described by an exponential function. The same data are plotted in figure 14(*b*), now as log $(\omega_{max}(\tau)/\omega_{max}(0))$ versus τ; the straight solid line has been fitted to the data by eye. The reasonable collapse of the data points onto the line confirms the conjecture that the decay is close to exponential, i.e.

$$\omega_{max}(\tau) = \omega_{max}(0)\, e^{-\beta\tau}. \tag{12}$$

For this particular experiment the slope of the straight line measures approximately $\beta = 1.8$.

It is not unreasonable to assume that the spin-down mechanism associated with the recirculation flow driven by the Ekman layer at the bottom is the major factor in the decay of the tripole vortex. For the decay of a monopolar, axisymmetric vortex in a free-surface rotating fluid it was found experimentally that the maximum swirl velocity of the vortex also decreases in an exponential fashion, but with an exponential coefficient $\beta \approx 1.1$ (see Kloosterziel & van Heijst 1991*b*). This value is somewhat larger than the value $\beta = 1$ derived by Greenspan & Howard (1963) for the

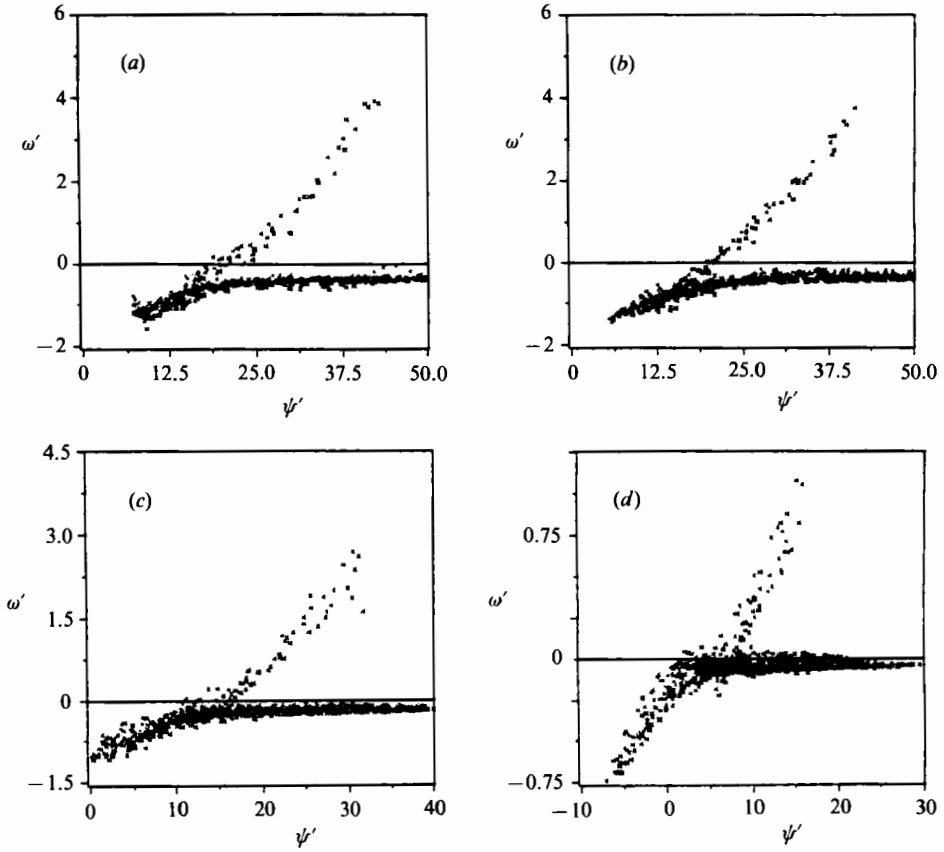

FIGURE 15. A typical evolution of the (ω', ψ') scatter plot during the tripole decay process is shown in (*a*)–(*d*). A correction has been made for the actual rotation speed $\dot{\Theta}$ of the tripole at the time of the photographic recording of the flow; this correction can be observed in the shift of the horizontal branch relative to the line $\omega' = 0$. The graphs correspond to subsequent stages in the decay process, viz. (*a*) $\tau \equiv t/T_E = 0.12$, (*b*) 0.14, (*c*) 0.26, and (*d*) 0.69, with $T_E = 174$ s. Experimental parameters: see figure 2.

linear spin-up or spin-down of fluid confined in a circular cylinder with a rigid lid. The deviation of the experimental result from the theoretically predicted value of the decay rate was attributed by Kloosterziel & van Heijst (1991*b*) to nonlinear effects. It appears that nonlinear effects account for the faster decay of tripoles too, but an analysis of the spin-down problem for vortices as complicated as tripoles has as-yet not been made.

In addition to the spin-down mechanism provided by the Ekman layer, the decrease of the tripole rotation speed and the decay of the relative flow within the tripolar structure may also be caused by the lateral entrainment of ambient fluid into the satellite vortices. This effect can be closely observed in the photographs presented in figures 1 and 3: the dyed fluid inside the satellites shows a spiral-like pattern, with undyed fluid 'sandwiched' in between. A notable feature is that the core vortex does not show this phenomenon; it is somehow much more shielded from penetration by the exterior fluid. The lateral entrainment – supposedly a viscous effect – apparently brings initially quiescent ambient fluid into the rotating tripole, and therewith contributes to a gradual slow-down of the rotation of the vortex

structure. As will be discussed in §4, the cross-sectional dimensions of the tripole, and in particular the separation distances between the centres of the satellites and the core vortex, show a gradual increase with time (see figure 18*b*). This 'widening' of the tripolar vortex clearly can be associated with the entrainment process. These features can also be observed in the evolution of the (ω, ψ) scatter plots of the tripole, as illustrated by figure 15. In the initial stage (figure 15*a*), the points show a clustering onto three well-defined branches, being the curved upper branch corresponding to the vortex core ($\omega' > \omega_{\text{corr}}$), the lower branch associated with the satellite vortices ($\omega' < \omega_{\text{corr}}$), and the horizontal branch ($\omega' = \omega_{\text{corr}}$) representing the irrotational exterior. Here ω' is the vorticity in the reference frame corotating with the tripole, i.e. $\omega' \equiv \omega + \omega_{\text{corr}}$, with ω the vorticity relative to the rotating tank (as derived from the digitized photographs), and ω_{corr} is the correction for the tripole rotation, i.e. $\omega_{\text{corr}} = -2\dot{\Theta}$, with $\dot{\Theta}$ the tripole rotation speed. Note that all the (ω, ψ) scatter plots presented in figure 15 have been corrected for the actual rotation of the tripole at the time the photographs were taken; this explains why the horizontal branch (representing the exterior) lies slightly below the line $\omega' = 0$. Owing to the diminishing rotation rate, this horizontal branch approaches the line $\omega' = 0$ more closely as time progresses.

In the subsequent stages the amplitude of the vorticity maximum ω_{max} is observed to decrease in comparison with the amplitude of the vorticity minimum $|\omega_{\text{min}}|$ found at the centre of the satellites, as is seen in figure 15(*b*, *c*). At later stages (see figure 15*d*), the amplitudes of vorticity extrema in the satellites and the central vortex become comparable in magnitude. The reason for this phenomenon lies in the sign of the vorticity. As discussed by Kloosterziel (1990) for the case of an axisymmetric vortex in a rotating fluid, the vorticity in the centre of a decaying vortex is governed by a Riccati-type equation. For a non-zero Rossby number this equation is not symmetric for changes in the sign of the relative vorticity, and it reveals that cyclonic vortices decay at a faster rate than their anticyclonic counterparts. Although the tripole has a much more complicated geometry, it may be expected that to some extent the same dynamics still apply to the individual sub-vortices (being core and satellites) of this vortex structure.

The scatter plot of the tripole in the later stages of its evolution shows the occurrence of a horizontal band between the intersections of the two main branches with the line $\omega' = \omega_{\text{corr}}$. This band corresponds to the flow in the regions between the central vortex and the satellites. Careful inspection of the dye patterns observed during this stage (cf. figure 1*f*) reveals that these regions contain undyed fluid, obviously originating from the irrotational exterior region. It thus appears that the lateral entrainment of ambient fluid, resulting in the 'widening' of the tripole, causes the branches of the core and the satellite vortices in the (ω, ψ)-plot to separate. Another feature that can be observed in the evolution of the (ω, ψ)-plot of the evolving tripole is the relaxation to linearity in both the (coinciding) satellite branches and the core branch.

It thus appears that, apart from a decrease in the magnitudes of velocities and vorticity, the decay is also characterized by a gradually changing distribution of these properties over the tripole structure, and also by a slightly changing shape of the vortex. In the light of this, it is worth considering the evolution of the velocity distributions along characteristic cross-sections through the tripole, as also shown in figure 5. For a typical experiment the time evolution of the velocity distribution along the major axis AA′ (see figure 5 for definition) is illustrated in figure 16. As mentioned before, these profiles are measured relative to the frame of the rotating

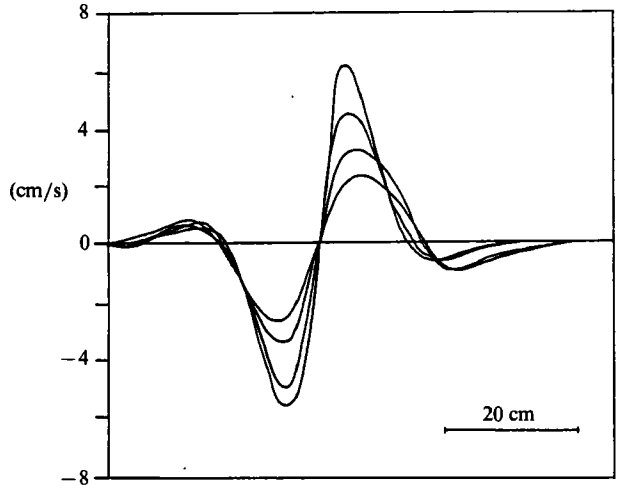

FIGURE 16. Graph showing the evolution of the flow profile along the main axis through a tripole (AA′ in figure 5). These profiles are taken from the tripole previously shown in figure 2, and were measured at (*a*) $t/T_E = 0.12$, (*b*) 0.26, (*c*) 0.41 and (*d*) 0.69, with $T_E = 175$ s. Experimental parameters: see figure 2.

tank; correction for the tripole rotation, however, would only have a slight effect on the velocity distribution. For the sequence shown here, the pertinent Rossby number (based on the maximum velocity, and its distance from the vortex centre) decreases from approximately 1.2 to 0.3 in the time interval $t = 0.12T_E$ to $0.69T_E$. One obvious feature visible in figure 16 is the significant decrease in the extrema of the velocity in the core vortex, whereas those in the satellite vortices hardly show any decrease during that time span. In addition, the evolving velocity distribution also indicates the widening of the tripole due to the lateral entrainment process, although in this particular case the widening shows some asymmetry: the zero at the right of the centre zero has shifted over a larger distance than the one at the left.

4. Comparison with a point-vortex model

It is clear from the results presented in §3 that the tripolar vortex is characterized by an essentially continuous vorticity distribution over three distinct regions that are initially close together but at later times farther apart. Monopolar and dipolar vortex structures in many different circumstances are also observed to have a continuous vorticity distribution (see Kloosterziel & van Heijst 1991*b*, and van Heijst & Flór 1989). Analytical models usually adopted for a description of these vortex structures are, for instance, some Gaussian model for isolated monopoles, and Lamb's dipole (see e.g. Lamb 1936 or Batchelor 1967) for the dipolar vortex. In both cases the vorticity is continuously distributed over the vortex structure. Because of its relatively recent discovery, such an analytical, distributed-vorticity model has not yet been developed for the isolated tripole as considered in the present paper. It is anticipated, however, that any (future) analytical tripole model with a continuous vorticity distribution will be considerably more difficult to construct than its monopolar and dipolar counterparts, owing to the intricate geometry of the tripolar vortex.

As a first step towards an analytical description of the flow, a model of a tripole

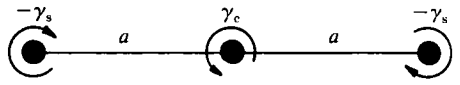

FIGURE 17. Schematic representation of the point-vortex model of the tripole.

will be considered in which the tripole consists of three symmetrically aligned point vortices of the appropriate signs and strengths. Point-vortex models – though rather crude simplifications of realistic vortex structures – have successfully been applied to describe the interaction of single-signed vortices; for example, the linear propagation of a dipolar vortex is nicely predicted by a model consisting of a pair of point vortices of equal but oppositely signed strengths. Also, the much more complicated mutual interaction of a large number of monopolar vortices (with non-zero circulation) in a two-dimensional flow can to a satisfactory degree be modelled by point vortices, as demonstrated in a numerical study by Benzi *et al.* (1987).

For the tripole, the obvious point-vortex model consists of a symmetric linear arrangement of three potential vortices as sketched in figure 17: the anticyclonic satellite vortices (with equal strengths γ_s) are placed at equal distances a from the central, cyclonic vortex (with strength γ_c). It can easily be verified that this vortex constellation rotates steadily, with angular speed

$$\Omega_{\text{tripole}} = \frac{2\gamma_c + \gamma_s}{4\pi a^2}. \tag{13}$$

The streamline pattern of the flow in a corotating frame of reference has been shown for the case $(\gamma_c, \gamma_s) = (2, -1)$ with $a = 1$ by Kloosterziel & van Heijst (1989). It has been mentioned in §3 that the tripole originates from an initially circular vortex with a zero net circulation: the area integral of the positive vorticity in the central core of the initial vortex is balanced by the integral of the negative vorticity distributed over the outer ring of the vortex. It might be expected, therefore, that the tripolar vortex – essentially formed by a reshaping of the outer ring of negative vorticity into the two satellite vortices – will still be characterized by a net circulation equal to zero, according to Kelvin's theorem, if viscous effects and deviations from the supposed two-dimensionality of the flow can be neglected. For the point-vortex model this would imply that the strengths ought to be chosen as $(\gamma_s, \gamma_c, \gamma_s) = (-\gamma, 2\gamma, -\gamma)$, so that – according to (13) – the angular speed of the model tripole would then be $3\gamma/(4\pi a^2)$.

In order to make any comparison between the 'real' tripole and its point-vortex idealization, one has to determine the strengths γ_c and γ_s, and also the separation distance a between the central vortex and its satellites. The strengths can be determined by numerical integration of the vorticity $\omega(\boldsymbol{x})$ over some area A (enclosed by a contour C) that represents one of the sub-vortices of the tripole:

$$\int_A \omega(\boldsymbol{x})\,\mathrm{d}A = \oint_C \boldsymbol{v}\cdot\mathrm{d}\boldsymbol{l} = \gamma, \tag{14}$$

with $\mathrm{d}\boldsymbol{l}$ an infinitesimal element of the closed contour C. The surface integral of the vorticity was estimated by calculating the conical volume with an elliptical or circular base defined by the $\omega = 0$ contour, and a cone height equal to max $(|\omega|)$. The continuous distribution of the vorticity within each of the sub-vortices is thus approximated by a linear function. A typical result of such calculations is shown graphically in figure 18(*a*): the strengths γ_{s1} and γ_{s2} of the satellite vortices, and the

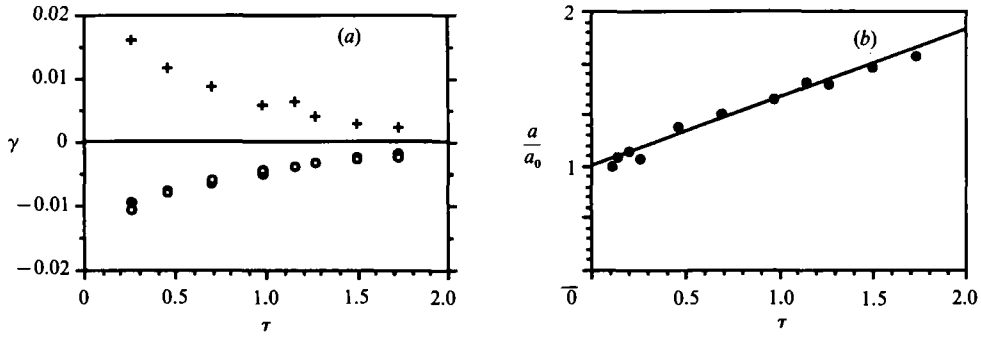

FIGURE 18. Graphical representations of (*a*) the vortex strengths γ_c, γ_{s1}, γ_{s2} (indicated by +, ○ and ●, respectively) and (*b*) the separation distance a between the core vortex and the satellites, as determined from the vorticity maps, for subsequent stages in the decay process. The data points in (*b*) have been normalized by the value a_0 of the separation distance as measured on the first photograph of the sequence. Experimental parameters: see figure 2.

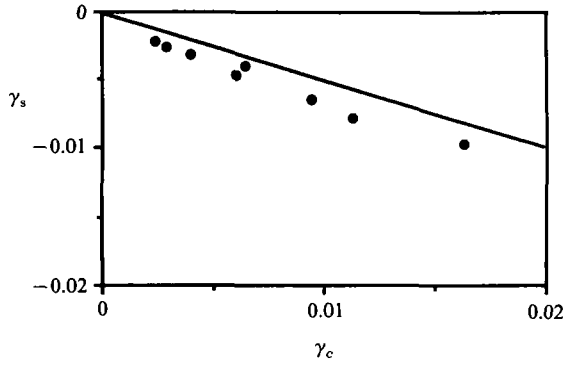

FIGURE 19. Graph showing the relative values of the circulations γ_c and γ_s (corresponding to the core and the satellites, respectively) in the decaying tripole. The data are the same as those presented in figure 18(*a*), although the average value $\gamma_s \equiv \frac{1}{2}(\gamma_{s1}+\gamma_{s2})$ of the satellite circulations has been plotted, rather than the individual values. The straight line represents the relationship $\gamma_s = -\frac{1}{2}\gamma_c$.

strength γ_c of the central vortex as determined at subsequent stages of the decay process are given as a function of the dimensionless time $\tau = t/T_E$. The decay of the vortex circulations is obvious.

The separation distances a_1 and a_2 between each of the satellite vortices and the tripole centre were determined by eye from the vorticity contour plots, and their average values $a = \frac{1}{2}(a_1+a_2)$ corresponding to the data points in figure 18(*a*) are presented graphically in figure 18(*b*). The data, which have been normalized by the value of a as measured on the first photograph of the sequence, suggest an approximately linear increase with time; the straight solid line has been fitted to the data by eye, and has for this experiment a slope of 0.66. As mentioned before, this 'widening' is attributed to the gradual entrainment of ambient fluid into the rotating tripole, as is visible in the dye patterns shown in figure 1.

It can be seen in figure 18(*a*) that in the course of the experiment the circulations γ_{s1} and γ_{s2} of the satellite vortices, while decreasing in magnitude, have approximately equal values – at least within the experimental accuracy – and this allows one to use their average value $\gamma_s \equiv \frac{1}{2}(\gamma_{s1}+\gamma_{s2})$ in the calculation of the tripole rotation speed according to (13). In order to check the conjecture that the net

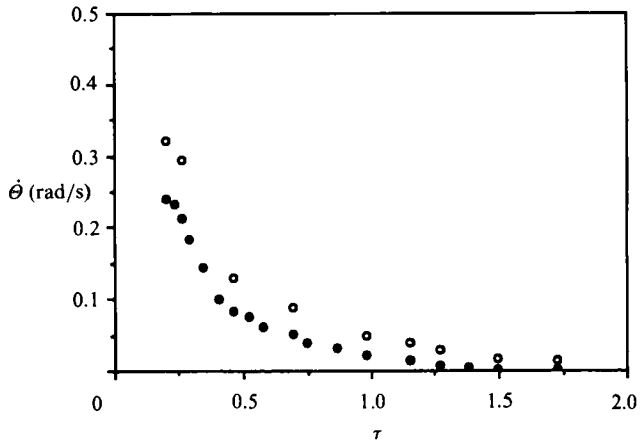

FIGURE 20. A comparison between the tripole rotation speed $\dot{\Theta}$ observed in the experiment and that predicted by the point-vortex model (13). The black dots represent the experimental data (cf. figure 9*b*), and the open circles represent the theoretical values of (13) based on the data given in figure 18. The calculation was carried out for a zero-circulation tripole $(-\gamma, 2\gamma, -\gamma)$, with $\gamma = \frac{1}{4}(\gamma_c + 2|\gamma_s|)$.

circulation of the tripole be zero, i.e. $\gamma_s = -\frac{1}{2}\gamma_c$, the values of γ_s were plotted versus the values of γ_c for the same times τ as in figure 18(*a*), and the result is presented in figure 19. For a correct interpretation of the graph it should be kept in mind that the values of γ_c and γ_s decrease with time. The solid line represents the conjectured relation $\gamma_s = -\frac{1}{2}\gamma_c$, from which the data appear to deviate systematically: the satellite vortices are systematically stronger than would be expected from Kelvin's circulation theorem. Because the departures from the relationship $\gamma_s = -\frac{1}{2}\gamma_c$ are rather marginal, the strength γ for a tripole indicated by the triplet $(-\gamma, 2\gamma, -\gamma)$ was calculated according to $\gamma = \frac{1}{4}(\gamma_c + 2|\gamma_s|)$. As mentioned before, the point-vortex model for this zero-circulation tripole predicts an angular velocity $3\gamma/(4\pi a^2)$, and the values calculated with the data given in figure 18 are presented graphically in figure 20, together with the observed rotation speed as given in figure 9.

It is obvious from this graph that, although the theoretically predicted values are systematically larger than the experimental data, the tendency for the rotation speed of the tripole to gradually decrease is represented fairly well by the point-vortex model. The discrepancy between the experimental data and the values predicted by the model can mainly be attributed to the crude estimation of the vortex strengths γ_c, γ_{s1} and γ_{s2} from the vorticity contour maps. As mentioned before, the surface integral (14) over the vorticity was approximated by calculating the volume of a cone with height max $(|\omega|)$ and a base defined by the $\omega = 0$ contour. This $\omega = 0$ contour usually has a rather erratic appearance (because the vorticity is calculated by differentiation of the flow field), implying that the base is ill-defined. Fitting with a circle or ellipse inevitably introduces substantial errors in the calculations of the γ-values. Moreover, the linear approximation, by taking a cone rather than a more realistic representation of $\omega(\boldsymbol{x})$ in A, adds to these errors. In addition to these approximations, the distances a_1 and a_2 between the satellites and the tripole centre are determined from the vorticity contour plots, assuming that the positions of the point vortices coincide with those of extremal vorticity. This assumption may hold for the centre vortex, but for the non-symmetric vorticity distributions of the satellites the centre of 'vortical gravity' does not in general

coincide with the position of the vorticity extremum, implying that some systematic errors in the estimation of the satellite separation distances are introduced in this way. Notwithstanding these inaccuracies in the approximation method, the results shown in figure 20 indicate a reasonably good agreement between the observed tripole rotation speed and the value predicted by the point-vortex model.

5. Stability

The stability problem of the tripole does not lend itself to an analytical treatment, for instance a normal-modes analysis, since a simple analytical expression reasonably representing a tripole with distributed vorticity has not been found yet. The coordinate-free characterization of the quasi-stationary tripoles, that is, the scatter plots, may play an important role in future nonlinear stability proofs of planar flows, but many technical problems still have to be overcome. The variety of functional relations between vorticity and stream function shown in figure 15, each corresponding to a quasi-stationary, stable tripole, indicates that extensive classes of nonlinearly stable tripoles exist, but proving this is as yet impossible.

The stability of the point-vortex tripole, briefly discussed in the previous section, is amenable to an analysis (see Aref 1979). An extensive analysis of this model shows that the point-vortex tripole with vanishing circulation is nonlinearly stable, i.e. for all small but finite perturbations the three vortices will remain close to each other (see Kloosterziel 1990). A model tripole with negative circulation, that is, with satellites each as strong as the central vortex, is found to split up – when perturbed – into a dipole that moves away, leaving behind a single vortex (see Morikawa & Swenson 1971).

The internal structure of the tripole is important as will be seen, and such finer details cannot be captured by a simple point-vortex model. For instance, in figure 21 the evolution of an unstable tripole is shown. In this particular case the central cyclonic vortex splits into two halves, each pairing with one of the satellites, thus leading to the formation of two dipoles that move away in opposite directions (this is reminiscent of the dipole splitting of anticyclones, as described by Kloosterziel & van Heijst 1989 but no tripole formed first in those cases). The scatter plot of the initial vortex that transformed into the tripole shown in figure 21 (*a*), is presented in figure 22. By comparing this initial condition with that of a stable tripole like shown in figure 11, a remarkable difference is observed, which probably accounts for the observed difference in stability behaviour. Both scatter plots show a vanishing gradient in the vorticity in the ring of negative vorticity, which is related to the formation of the satellites, but in figure 22 the gradient also appears to vanish close to the centre of the vortex, i.e. at the tip of the upper branch. Although a proof of instability necessarily involves the construction of a growing mode, it is a strong hint that the central vortex is itself unstable, which, with hindsight, is seen to be true.

Another important difference between the scatter plot of a vortex leading to the formation of a stable tripole (figure 11) and the one leading to an unstable tripole (e.g. figure 22) lies in the ratio of the negative and positive vorticity amplitudes. As remarked before, the initial monopolar vortex has a core of positive vorticity, surrounded by a band of negative vorticity. It was found in an analytical study (Flierl 1988) that the stability behaviour of piecewise-constant-vorticity vortices strongly depends on their vorticity distribution, i.e. on the width of the outer ring of negative vorticity relative to the core diameter, and the ratio of the negative and positive vorticity amplitudes. Although this approach is rather approximate (the

(a)

(b)

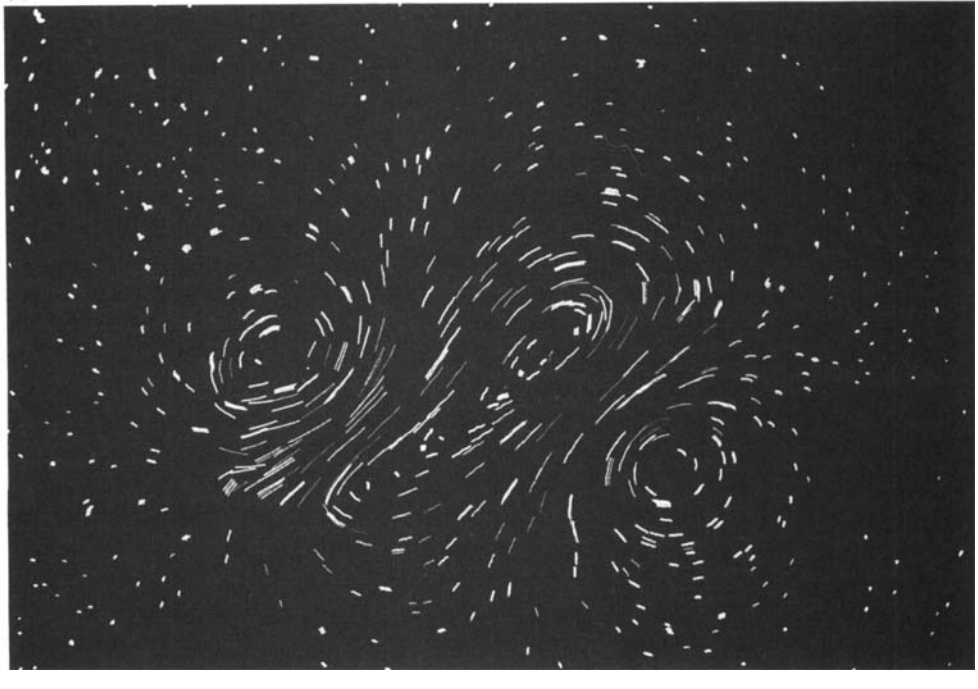

FIGURE 21 (a, b). For caption see facing page.

(*c*)

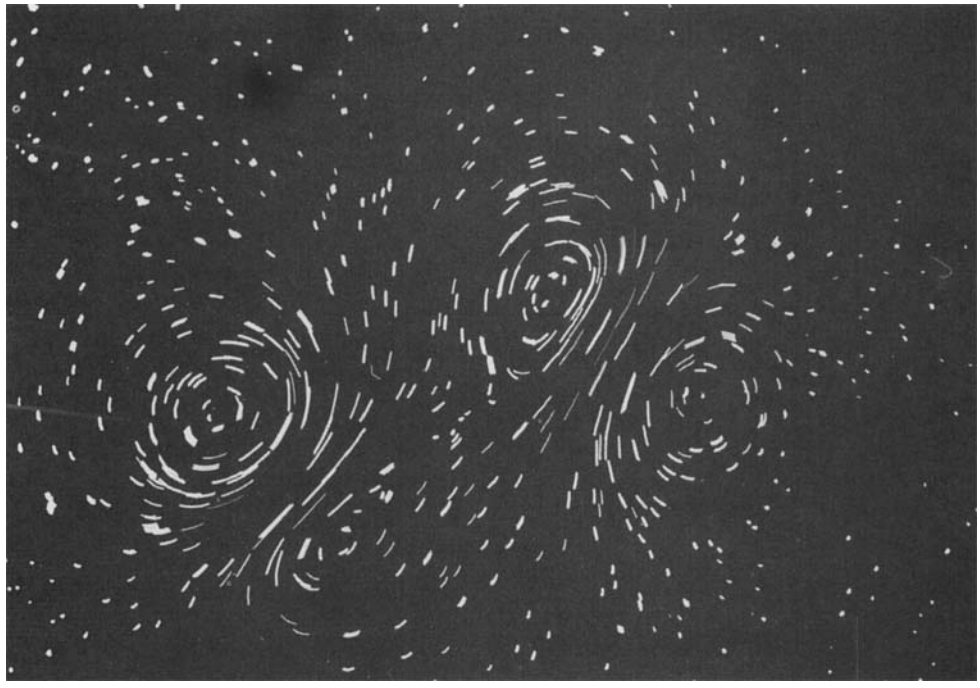

(*d*)

FIGURE 21. Streakline photographs showing the evolution of an unstable tripole. The photographs were taken at times (*a*) $t = 2.7T$, (*b*) $3.3T$, (*c*) $3.9T$ and (*d*) $4.5T$ after lifting the cylinder, with $T = 6.4$ s the rotation period of the turntable. This vortex was created by stirring cyclonically in a cylinder with a diameter $2R_0 = 20$ cm. The average water depth was $\bar{H} = 17.6$ cm.

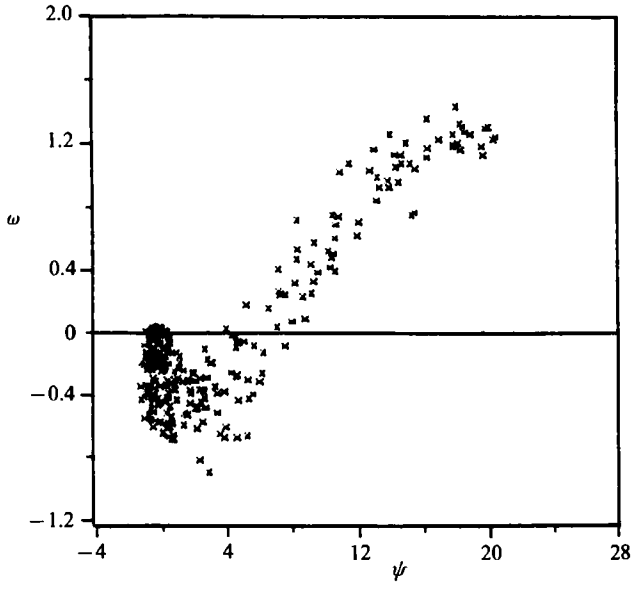

FIGURE 22. Scatter plot of the cyclonic stirring vortex that eventually turned into the unstable tripole shown in figure 21.

continuous distribution being modelled by a discrete distribution of constant positive vorticity and constant negative vorticity), some of its results have turned out to be in accordance with laboratory observations of unstable vortices (Kloosterziel & van Heijst 1991*a*). The scatter plot of the vortex that eventually became unstable (figure 22) reveals an amplitude ratio close to one, which implies – according to Flierl's (1988) results – that the vortex is more unstable than its counterpart with a smaller amplitude ratio. Following the sequence of respective events (compare figures 2 and 21), this appears to be true. Finally, in figure 23 the evolution of the vorticity distribution as determined by digitizing the streakline photographs of figure 21 is shown.

6. Conclusions

The tripolar vortex is a relatively novel feature in fluid mechanics, and although a number of its properties have been investigated recently in numerical studies (Legras *et al.* 1988; Carton *et al.* 1989; Polvani & Carton 1990), the laboratory experiments described in this paper are the first in which the dynamical properties of 'real' tripoles were measured. The tripole consists of three aligned patches of distributed vorticity of alternate signs, and the structure rotates as a whole about the centre of the core vortex. In the previous sections of the paper it was shown that in a rotating fluid the tripole vortex can emerge as a stable end-product of an unstable cyclonic monopolar vortex. The initial axisymmetric vortex consists of a core of cyclonic relative vorticity surrounded by a ring of anticyclonic relative vorticity. During the transformation into the tripole structure, the vorticity is observed to be redistributed in such a way that eventually the negative and the positive vorticity are concentrated in the two satellite vortices and the central vortex, respectively. This process of vorticity redistribution (or of other material properties of the flow) is nicely

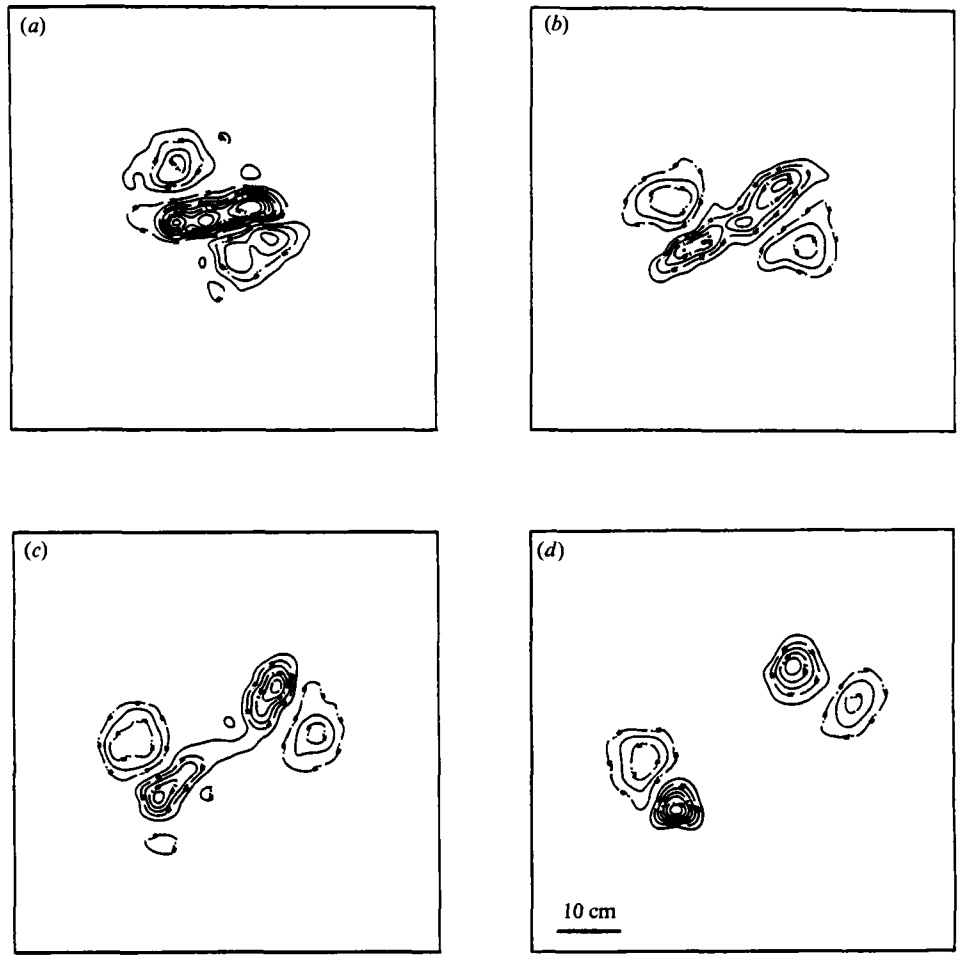

FIGURE 23. Sequence of vorticity contour plots illustrating the evolution of an unstable tripole. The plots were obtained by digitizing the streakline photographs presented in figure 21, and for experimental parameters one is referred to the caption of that figure.

illustrated by the experiments shown in figure 3, in which the core and the outer ring of the initial vortex were coloured with different dyes.

Digitization of streakline photographs yielded quantitative information about the flow in the subsequent stages of the tripole formation process. This technique revealed that the tripolar vortex is characterized by an essentially continuous distribution of the vorticity, as can be clearly seen both on the vorticity contour plots (see figure 6*a*) and the scatter plots of vorticity versus stream function (see figure 12). Owing to its rather complicated geometry, no analytical model of the tripolar vortex (with a continuous distribution of vorticity) has been formulated yet. An over-simplifying point-vortex model, in which the distributed vorticity of the core and its satellites are thought to be concentrated in three potential vortices, is capable of capturing one of the tripole's prominent features, viz. the rotation of its alignment axis (see figure 20).

The decay of the tripole, as apparent from its decreasing rotation speed and the

decrease of relative flow and vorticity, is a complicated process, being partially due to the spin-up/spin-down mechanism provided by the bottom Ekman layer, partially caused by lateral entrainment of ambient fluid into the satellite vortices.

The calculations of the interpolated flow fields and related quantities were carried out by the use of software kindly provided by Drs Joël Sommeria, Than Nguyen Duc and Mathieu Mory (Madylam, Institut de Mécanique de Grenoble, France) and their cooperation is greatly appreciated. We are also much indebted to Piet Jonker for his help in adapting the numerical code to the mainframe computer of the University of Utrecht. One of us (R.C.K.) gratefully acknowledges financial support from the working group on Meteorology and Physical Oceanography (MFO) of the Netherlands Organization of Scientific Research (NWO).

REFERENCES

AREF, H. 1979 Motion of three vortices. *Phys. Fluids* **22**, 393–400.

BATCHELOR, G. K. 1967 *An Introduction to Fluid Dynamics*. Cambridge University Press, 615 pp.

BENZI, R., PATARNELLO, S. & SANTANGELO, P. 1987 On the statistical properties of two-dimensional decaying turbulence. *Europhys. Lett.* **3**, 811–818.

BENZI, R., PATARNELLO, S. & SANTANGELO, P. 1988 Self-similar coherent structures in two-dimensional decaying turbulence. *J. Phys.* A: *Math. Gen.* **21**, 1221–1237.

CARNEVALE, G. F., KLOOSTERZIEL, R. C. & HEIJST, G. J. F. VAN 1991 Propagation of barotropic vortices over topography in a rotating tank. *J. Fluid Mech.* (submitted).

CARTON, X. J., FLIERL, G. R. & POLVANI, L. M. 1989 The generation of tripoles from unstable axisymmetric isolated vortex structures. *Europhys. Lett.* **9**, 339–344.

CHANDRASEKHAR, S. 1961 *Hydrodynamic and Hydromagnetic Stability*. Oxford University Press, 654 pp.

DRAZIN, P. G. & REID, W. H. 1981 *Hydrodynamic Stability*. Cambridge University Press, 527 pp.

FLIERL, G. R. 1988 On the instability of geostrophic vortices. *J. Fluid Mech.* **197**, 349–388.

GREENSPAN, H. P. & HOWARD, L. N. 1963 On a time-dependent motion of a rotating fluid. *J. Fluid Mech.* **17**, 385–404.

HASEGAWA, A. 1985 Self-organization processes in continuous media. *Adv. Phys.* **34**, 1–42.

HEIJST, G. J. F. VAN & FLÓR, J. B. 1989 Dipole formation and collisions in a stratified fluid. *Nature* **340**, 212–215.

HEIJST, G. J. F. VAN & KLOOSTERZIEL, R. C. 1989 Tripolar vortices in a rotating fluid. *Nature* **338**, 569–571.

HOLTON, J. R. 1979 *An Introduction to Dynamic Meteorology* (2nd edn.). Academic, 391 pp.

IKEDA, M. 1981 Instability and splitting of mesoscale rings using a two-layer quasi-geostrophic model on an *f*-plane. *J. Phys. Oceanogr.* **11**, 987–998.

KLOOSTERZIEL, R. C. 1990 Barotropic vortices in a rotating fluid. Ph.D. thesis, University of Utrecht, The Netherlands.

KLOOSTERZIEL, R. C. & HEIJST, G. J. F. VAN 1989 On tripolar vortices. In *Mesoscale/Synoptic Coherent Structures in Geophysical Turbulence* (ed. J. C. J. Nihoul & B. M. Jamart), pp. 609–625. Elsevier.

KLOOSTERZIEL, R. C. & HEIJST, G. J. F. VAN 1991*a* An experimental study of unstable barotropic vortices in a rotating fluid. *J. Fluid Mech.* **223**, 1–24.

KLOOSTERZIEL, R. C. & HEIJST, G. J. F. VAN 1991*b* The evolution of stable barotropic vortices in a rotating free-surface fluid. *J. Fluid Mech.* (submitted).

LAMB, H. 1936 *Hydrodynamics* (6th edn.) Cambridge University Press, 738 pp.

LEGRAS, B., SANTANGELO, P. & BENZI, R. 1988 High-resolution numerical experiments for forced two-dimensional turbulence. *Europhys. Lett.* **5**, 37–42.

LEITH, C. E. 1984 Minimum enstrophy vortices. *Phys. Fluids* **27**, 1388–1395.

McWilliams, J. C. 1984 The emergence of isolated coherent vortices in turbulent flow. *J. Fluid Mech.* **146**, 21–43.

Morikawa, G. K. & Swenson, E. V. 1971 Interacting motion of rectilinear geostrophic vortices. *Phys. Fluids* **14**, 1058–1073.

Nguyen Duc, J. M. & Sommeria, J. 1988 Experimental characterization of steady two-dimensional vortex couples. *J. Fluid Mech.* **192**, 175–192.

Polvani, L. M. & Carton, X. J. 1990 The tripole: a new coherent vortex structure of incompressible two-dimensional flows. *Geophys. Astrophys. Fluid Dyn.* **51**, 87–102.

Sadourny, S. 1985 Quasi-geostrophic turbulence: an introduction. In *Turbulence and Predictability in Geophysical Fluid Dynamics and Climate Dynamics* (ed. M. Ghill), pp. 133–158. North-Holland.

Stern, M. E. 1987 Horizontal entrainment and detrainment in large-scale eddies. *J. Phys. Oceanogr.* **17**, 1688–1695.

Swenson, M. 1987 Instability of equivalent barotropic riders. *J. Phys. Oceanogr.* **17**, 492–506.

Taylor, J. B. 1974 Relaxation of toroidal plasma and generation of reverse magnetic fields. *Phys. Rev. Lett.* **33**, 1139–1141.